Scientific Contributions Oil & Gas, Vol. 49. No. 2, June: 353 - 375

SCIENTIFIC CONTRIBUTIONS OIL AND GAS

Testing Center for Oil and Gas
LEMIGAS

Journal Homepage:http://journal.lemigas.esdm.go.id
ISSN: 2089-3361, e-ISSN: 2541-0520

Seismic-Based Reservoir Characterization of The Lower Arang Formation in West Natuna Basin Using Acoustic Impedance Inversion and Seismic Attributes

Hakim Afif Putra[1], Edi Sanjaya, Suwondo[1], Muhammad Nafian, Praditiyo Riyadi[1], and Widi Atmoko[2]

[1]Department of Physics, Faculty of Science and Technology, Syarif Hidayatullah State Islamic University Jakarta,
Ir. H. Juanda Street, Ciputat, South Tangerang, Banten 15412, Indonesia.

[2]Patra Nusa Data,
Taman Tekno BSD, G2 Block No. 1, Sector XI, Setu District, Tangerang Regency, Banten 15314, Indonesia.

Corresponding author: Edi Sanjaya (edi.sanjaya@uinjkt.ac.id)

Manuscript received: February 19th, 2026; Revised: March 27th, 2026
Approved: May 05th, 2026; Available online: June 15th, 2026; Published: June 16th, 2026.

ABSTRACT - Reservoir characterization is a critical stage in hydrocarbon potential evaluation, particularly for heterogeneous sandstone reservoirs. This study aims to characterize the reservoir of the Lower Arang Formation in The West Natuna Basin using acoustic impedance (AI) inversion and seismic attributes. This study used seismic and well log data integrated through a well–seismic tie to ensure consistency between the time and depth domains. Model-based AI inversion is used to determine the subsurface impedance distribution, while seismic attributes, including Root Mean Square (RMS) amplitude, variance, envelope, and sweetness, are analyzed to identify lithological variations and reservoir property indications. Petrophysical analysis incorporating Archie's equation is used to estimate water saturation (Sw) and identify reservoir fluid types. The results show that zones with relatively low AI values are strongly correlated with porous sandstone intervals in the Lower Arang Formation. Water saturation estimation at Apip-1 (Sw ≈ 0.35 –0.50) suggested a transitional interval with hydrocarbon indication, while Apip-2 (Sw ≈ 0.40–0.50) indicated a comparable transitional zone. Furthermore, the integration of inversion results with seismic attributes, supported by quantitative amplitude threshold analysis, improves the delineation of lateral reservoir distribution and enhanced the reliability of reservoir characterization. Overall, this integrates workflow provides an effective methodology for reservoir evaluation in basins with similar geological characteristics.

Keywords: acoustic impedance, seismic attributes, reservoir characterization, Lower Arang Formation, West Natuna Basin, water saturation, Archie's equation

How to cite this article:

Hakim Afif Putra, Edi Sanjaya, Suwondo, Muhammad Nafian, Praditiyo Riyadi, and Widi Atmoko, 2026, Seismic-Based Reservoir Characterization of The Lower Arang Formation in West Natuna Basin Using Acoustic Impedance Inversion and Seismic Attributes, Scientific Contributions Oil and Gas, 49 (2) pp. 353-375. DOI org/10.29017/scog.v49i2.2065.

INTRODUCTION

Reservoir characterization is an essential aspect in hydrocarbon exploration and field development, providing quantitative insight into reservoir geometry, lithology, and petrophysical properties. In clastic systems, particularly sandstone reservoirs, heterogeneity in grain composition, diagenesis, and pore structure often leads to significant uncertainty in predicting reservoir quality and spatial distribution. To reduce this uncertainty, the integration of seismic and well log data has been widely recognized as an effective method for improving subsurface characterization and predictability. This integration is essential because seismic data offer extensive lateral coverage, while well log data provides high-resolution vertical information, enabling more reliable reservoir evaluation (Asquith & Krygowski 2004; Rider & Kennedy 2011).

Despite the advantages, conventional seismic interpretation based only on reflection amplitude often fails to capture detailed rock property variations, particularly in geologically complex settings. Similar amplitude responses can also originate from different combinations of lithology, porosity, and fluid content, leading to ambiguity in interpretation. To address this limitation, seismic inversion methods have been widely developed to transform reflection data into quantitative elastic parameters, such as acoustic impedance (AI), which are more directly related to rock physical properties (Aki & Richards 2002; Latimer et al., 2000). AI is defined as the product of P-wave velocity (Vp) and bulk density (ñ), providing a physically meaningful parameter that can be correlated with porosity and lithology variations in sandstone reservoirs (Mavko et al., 1998).

In addition to inversion methods, seismic attribute analysis has proven effective in enhancing stratigraphic and structural interpretation. Various attributes such as Root Mean Square (RMS) amplitude, variance, envelope, and sweetness are widely used to identify lateral discontinuities, reflector continuity, and amplitude anomalies associated with reservoir development (Taner et al., 1979; Chopra & Marfurt 2005; 2007). Therefore, integration of AI inversion and seismic attributes offers a robust framework for improving reservoir delineation and reducing interpretation uncertainty (Castagna 2003). Recent studies in Indonesian basins have shown that multiattribute methods, when combined with comprehensive petrophysical analysis including water saturation estimation, significantly improve the reliability of reservoir characterization conclusions (Yusuf et al., 2016; Antariksa et al., 2023). For example, West Natuna Basin is an important hydrocarbon-producing region in Indonesia, characterized by syn-rift to post-rift depositional systems and complex structural evolution (Doust & Noble 2008; Surjono et al., 2023).

In this basin, the Lower Arang Formation is recognized as a potential clastic reservoir predominantly composed of sandstone with variable petrophysical characteristics. However, heterogeneity in the Lower Arang interval poses challenges in delineating reservoir geometry and identifying zones with favorable reservoir quality. Although previous studies have addressed stratigraphic and sedimentological aspects of the formation (Paskah et al., 2018; Rachmad et al., 2017), there is limited information on the quantitative reservoir characterization integrating seismic inversion, attribute analysis, and fluid identification from petrophysical analysis. Machine

-learning and advanced geophysical methods have started to complement conventional methods in similar basin settings (Haris et al., 2021; Verma & Bhattacharya 2025), showing the value of robust quantitative workflows.

Based on the description above, this study aims to characterize the reservoir of the Lower Arang Formation using model-based AI inversion integrated with seismic attribute analysis and petrophysical interpretation. The analysis includes estimation of water saturation using Archie's equation and quantitative attribute threshold analysis. This study integrates well log data, inversion results, and attribute interpretation to improve understanding of lateral and vertical reservoir distribution within the Lower Arang Formation. Furthermore, the results are anticipated to provide valuable insight into the applicability of the integrated workflow for reservoir evaluation in similar syn-rift basin settings.

METHODOLOGY

Methodological implementation in this study was supported by several geophysical software packages. Petrel 2018 was used for seismic data visualization, horizon picking, fault interpretation, time structure mapping, seismic attribute extraction, and reservoir polygon delineation. Hampson–Russell 10.1 was used for well–seismic tie analysis, statistical wavelet extraction, synthetic seismogram generation, initial impedance model construction, and model-based acoustic impedance inversion. The use of these software packages enabled the integration of 3D seismic data, well log data, interpreted horizons, and inversion results to support reservoir characterization of the Lower Arang Formation.

Study workflow

This study was carried out using an integrated seismic reservoir characterization workflow combining well log analysis, seismic interpretation, AI inversion, and seismic attribute evaluation. The workflow started with data preparation and regional geological assessment, followed by well–seismic tie calibration to ensure consistency between depth and time domains. Structural interpretation, including horizon and fault picking, was performed to establish the structural framework of the Lower Arang Formation.

Model-based AI inversion was conducted using well-derived impedance logs as constraints. Seismic attributes, including RMS amplitude, variance, envelope, and sweetness, were extracted along the target horizon to enhance lateral reservoir delineation. Subsequently, the integration of inversion results and attribute analysis was used to interpret reservoir geometry and distribution. The complete workflow implemented in this study is shown in Figure 1.

Well–seismic tie

Well–seismic tie was performed to establish a reliable relationship between depth-based well log and time-domain seismic data before inversion. Synthetic seismograms were generated from sonic (DT) and density (RHOB) logs by calculating reflection coefficients and convolving with an extracted wavelet, following the convolutional model of seismic reflection (Aki and Richards, 2002). A statistical wavelet extraction with a zero-phase assumption was applied to optimize the alignment between synthetic and observed seismic traces (Latimer et al., 2000).

Correlation analysis between synthetic seismograms and seismic traces showed satisfactory matching at both wells. The correlation coefficient at Well Apip-1 reached approximately 0.93, while Well Apip-2 was approximately 0.97. These values indicate good calibration quality, confirming that the seismic data are suitable for further structural interpretation and AI inversion.

Horizon picking and fault interpretation

After satisfactory well–seismic calibration, seismic interpretation was conducted to define the structural framework of the Lower Arang Formation. Horizon picking focused on identifying the top of the Lower Arang Top Sand interval based on reflector continuity and correlation with well markers. Subsequently, fault interpretation was performed to delineate structural discontinuities and establish compartmentalization in the study area. The interpreted horizons and

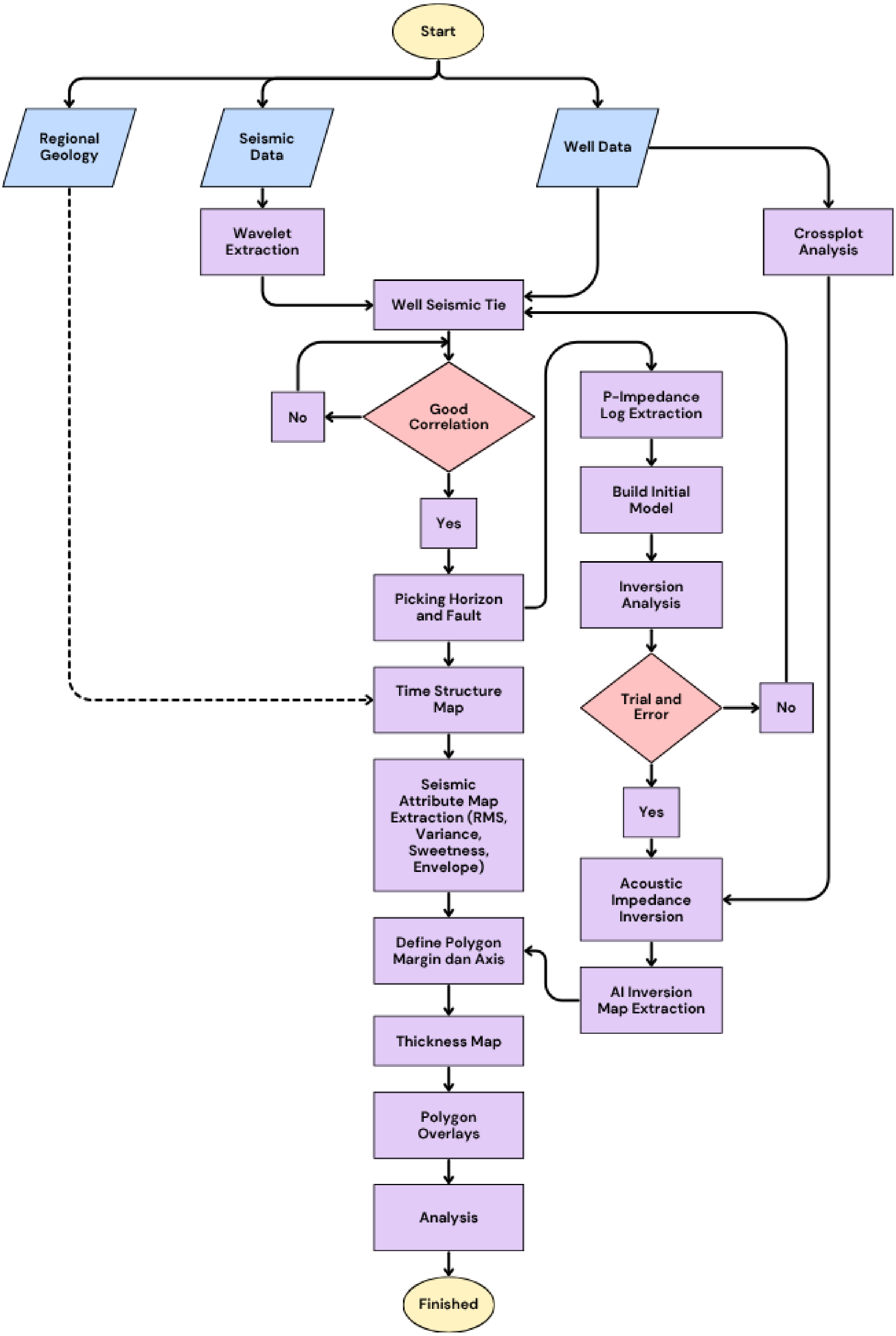

Figure 1. Workflow of seismic reservoir characterization applied in this study, showing the integration of well log analysis, well – seismic tie, seismic interpretation, acoustic impedance inversion, seismic attribute extraction, and reservoir delineation.

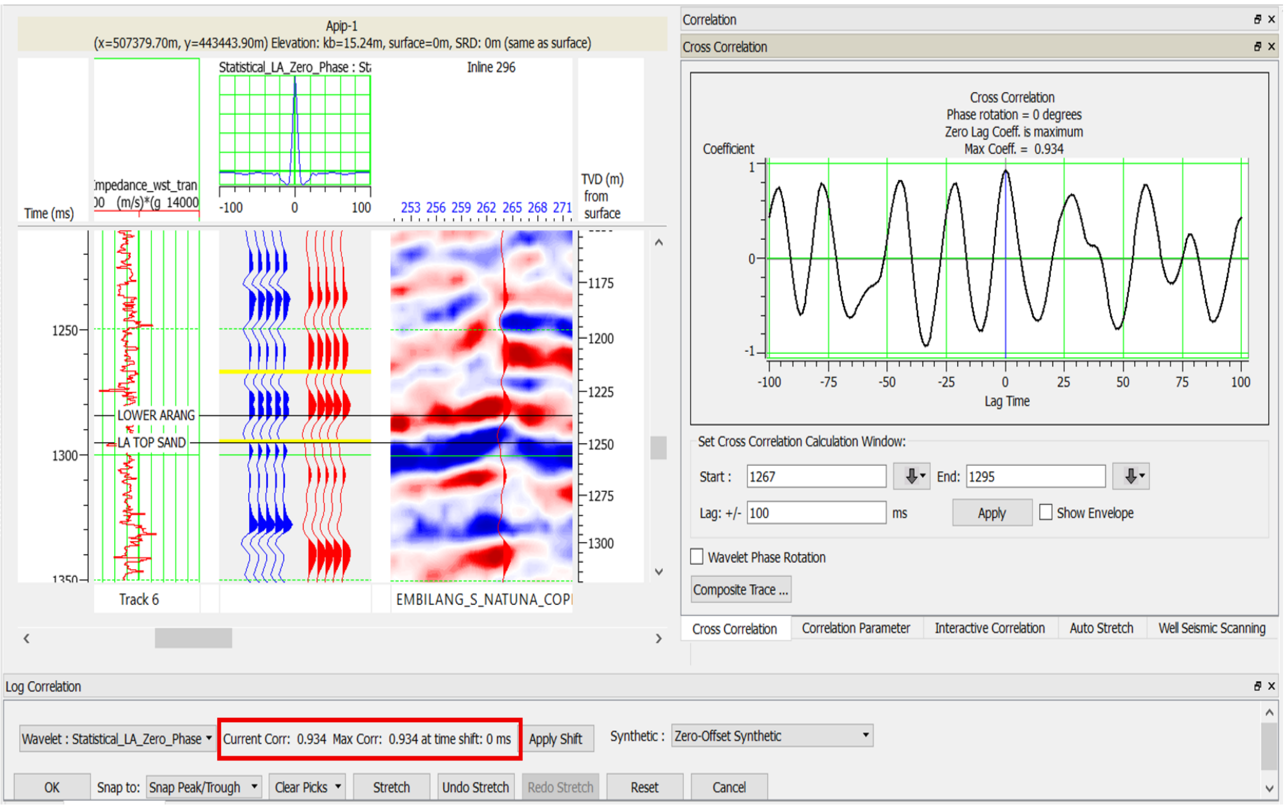

Figure 2. Well – seismic tie result at Well Apip-1 showing a good correlation between the synthetic seismogram and seismic trace, with a correlation coefficient of approximately 0.93, indicating reliable time – depth calibration for subsequent acoustic impedance inversion.

faults were integrated to generate a time structure map representing the two-way travel time (TWT) distribution of the target interval. This structural framework provides the geometric basis for further attribute analysis and AI inversion.

Seismic attribute extraction

Seismic attribute extraction was performed to enhance the delineation of lateral reservoir variations in the Lower Arang Formation. Attributes sensitive to amplitude and energy characteristics were selected, including RMS amplitude, variance, envelope, and sweetness. These attributes are widely applied in reservoir characterization because of the ability to emphasize reflector continuity, structural discontinuities, and lithological contrasts (Chopra & Marfurt 2005; Taner et al., 1979).

RMS amplitude represents the reflection energy in a specified time window, which is commonly associated with AI contrasts. The variance attribute shows lateral discontinuities that may indicate faults or facies changes. Envelope measures instantaneous signal energy independent of polarity, while sweetness combines amplitude and frequency information, showing sensitivity to porous sandstone development. In this study, all attributes were extracted along horizon slices corresponding to the Lower Arang Top Sand interval to identify lateral heterogeneity and support reservoir delineation.

Acoustic impedance inversion

AI inversion was performed using a model-based method to transform seismic reflection data into quantitative rock property information. Acoustic impedance (AI) is defined as the product of P-wave velocity and bulk density, as shown in Equation 1:

$$AI = V_p \times \rho \tag{1}$$

where Vp is P-wave velocity, and ñ is bulk density. Variations in AI across geological boundaries generate seismic reflections according to the convolutional model (Aki & Richards 2002). Since AI is directly related to lithology and porosity, it provides a more physically meaningful parameter for reservoir characterization compared to conventional amplitude interpretation (Latimer et al., 2000; Mavko et al., 1998).

Initial impedance models were constructed from well log-derived impedance values and constrained by interpreted horizons to preserve stratigraphic consistency. Specifically, model-based inversion was selected because of the ability to incorporate a priori geological information, improving vertical resolution and stability compared to unconstrained inversion approaches (Hampson et al., 2005). The inversion process was performed iteratively to minimize the mismatch between synthetic and observed seismic traces.

RESULT AND DISCUSSION

Well log response and reservoir identification

Well log analysis was conducted to characterize the Lower Arang Top Sand interval in Apip-1 and Apip-2 using quality-controlled log data. The interpretation integrated gamma ray (GR), spontaneous potential (SP), resistivity (ILD, LLD, LLS, MSFL), density (RHOB), neutron porosity (NPHI), caliper, and density correction (DRHO) logs to evaluate lithology, porosity, and reservoir quality. Log interpretation followed the established petrophysical principles for clastic reservoir evaluation (Asquith & Krygowski 2004; Rider & Kennedy 2011).

In Apip-1, the Lower Arang Top Sand interval was characterized by relatively low GR values (approximately 50–55 API), indicating low shale content and suggesting sandstone dominance. SP curve showed consistent deflection relative to the shale baseline, implying permeable formations. Stable caliper readings of approximately 12 inches indicated good borehole conditions and reliable log measurements. Furthermore, resistivity logs showed clear shallow–deep separation, with ILD values of approximately 25–30 ohm·m and LLD–LLS values around 60 ohm·m, which indicated permeable zones containing relatively resistive fluids. RHOB values ranging from 2.05 to 2.10 g/cm³ and NPHI values between 0.25 and 0.30 v/v

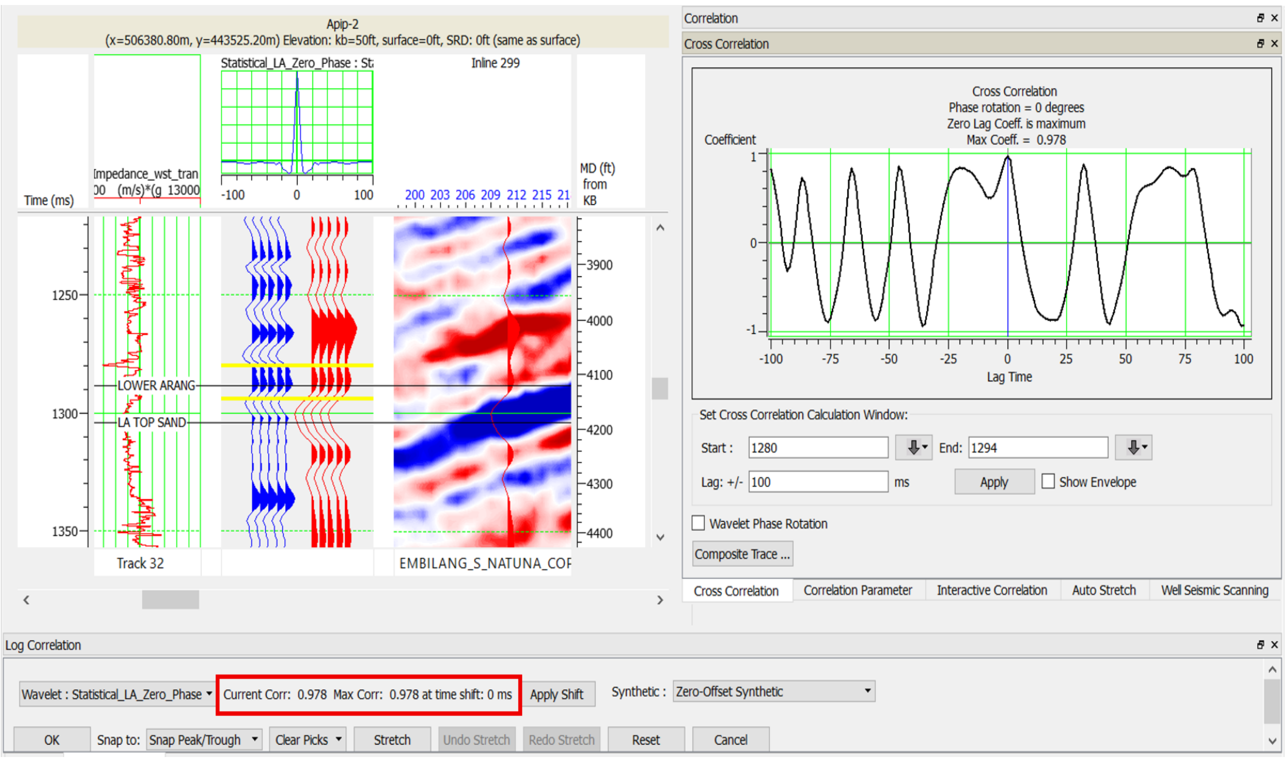

Figure 3. Well - seismic tie result at Well Apip-2 showing a strong correlation between the synthetic seismogram and seismic trace, with a correlation coefficient of approximately 0.97, indicating reliable time - depth calibration for subsequent acoustic impedance inversion.

suggested moderate to good porosity. DRHO values close to zero further confirm measurement reliability.

Based on the results obtained in Apip-2, the target interval showed slightly higher GR values (55–60 API), suggesting minor shale admixture compared to Apip-1, but consistent with sandstone lithology. SP responses and caliper stability indicated comparable permeability and borehole conditions. Resistivity values are lower than those observed in Apip-1 (ILD approximately 14–15 ohm·m). This indicates differences in fluid saturation or local compaction rather than significant lateral facies change. RHOB and NPHI responses remained consistent with moderate to good porosity.

Petrophysical cutoff thresholds applied for net sand identification included GR < 65 API (or shale volume Vsh < 0.5) and NPHI > 0.15 v/v (effective porosity ö > 15%). These cutoffs are consistent with regional clastic reservoir standards for West Natuna Basin (Asquith and Krygowski, 2004; Yusuf et al., 2016).

Water saturation (Sw) was estimated using Archie's equation (Archie 1942), as shown in Equation 2:

$$S_w{}^n = (a \times R_w) \,/\, (\varphi^{m} \times R_t) \qquad (2)$$

where Rw is formation water resistivity (estimated at approximately 0.05 ohm·m based on regional salinity data for West Natuna Basin), Rt is true formation resistivity (ILD), ö is effective porosity derived from NPHI-RHOB crossplot, and Archie parameters a = 1, m = 2, n = 2 are assumed as standard values for clean sandstone (Asquith & Krygowski 2004; Schlumberger 1989).

At Apip-1, estimated Sw values in the Lower Arang Top Sand interval ranged from approximately 0.35 to 0.50. When integrated with ILD readings of 25–30 ohm·m exceeding the expected Rw-derived background resistivity, these values suggest a transitional interval with hydrocarbon indication. SP deflection pattern and resistivity log character are consistent with a permeable reservoir interval. At Apip-2, estimated Sw values ranged from approximately 0.40 to 0.50. However, corresponding ILD values of 14–15 ohm·m are lower than those at Apip-1, suggesting comparable fluid saturation conditions with reduced resistivity response. This difference is attributed to local variations such as compaction effects or salinity variation rather than a fundamentally separate fluid type. Despite the variations, the relatively similar Sw range between the two wells provides an important context for interpreting AI and seismic attribute distributions across the study area.

The integrated log response confirmed that the Lower Arang Top Sand interval represented a sandstone reservoir with favorable petrophysical characteristics. Furthermore, Apip-1 showed more favorable fluid indicators compared to Apip-2. These log-based interpretations provide a reliable reference for subsequent AI analysis and seismic attribute correlation.

Acoustic impedance and porosity sensitivity analysis

A sensitivity analysis was conducted using crossplots between P-impedance and NPHI in the Lower Arang Top Sand interval to evaluate the relationship between AI and porosity. The crossplot analysis also provided the quantitative basis for defining the impedance cutoff used in subsequent reservoir delineation, ensuring that polygon boundaries were data-driven rather than qualitatively inferred. In Apip-1, P-impedance versus NPHI crossplot showed a clear inverse trend. Zones characterized by relatively low P-impedance values (approximately 5,200–6,200 m/ s·g/cc) and higher NPHI values (0.26–0.34 v/v) were interpreted as sandstone intervals with better reservoir quality. In comparison, impedance values exceeding approximately 6,300 m/s·g/cc corresponded to more compact, lower-porosity rocks. This interpretation is supported by GR color-coding, as lower impedance clusters coincide with lower GR values, indicating cleaner sandstone intervals. A comparable inverse relationship was observed in Apip-2, with P-impedance values ranging from approximately 5,300–6,200 m/s·g/cc corresponding to NPHI values between 0.28 and 0.35 v/v. Slightly higher impedance distributions relative to Apip-1 showed local compaction differences or minor facies variation.

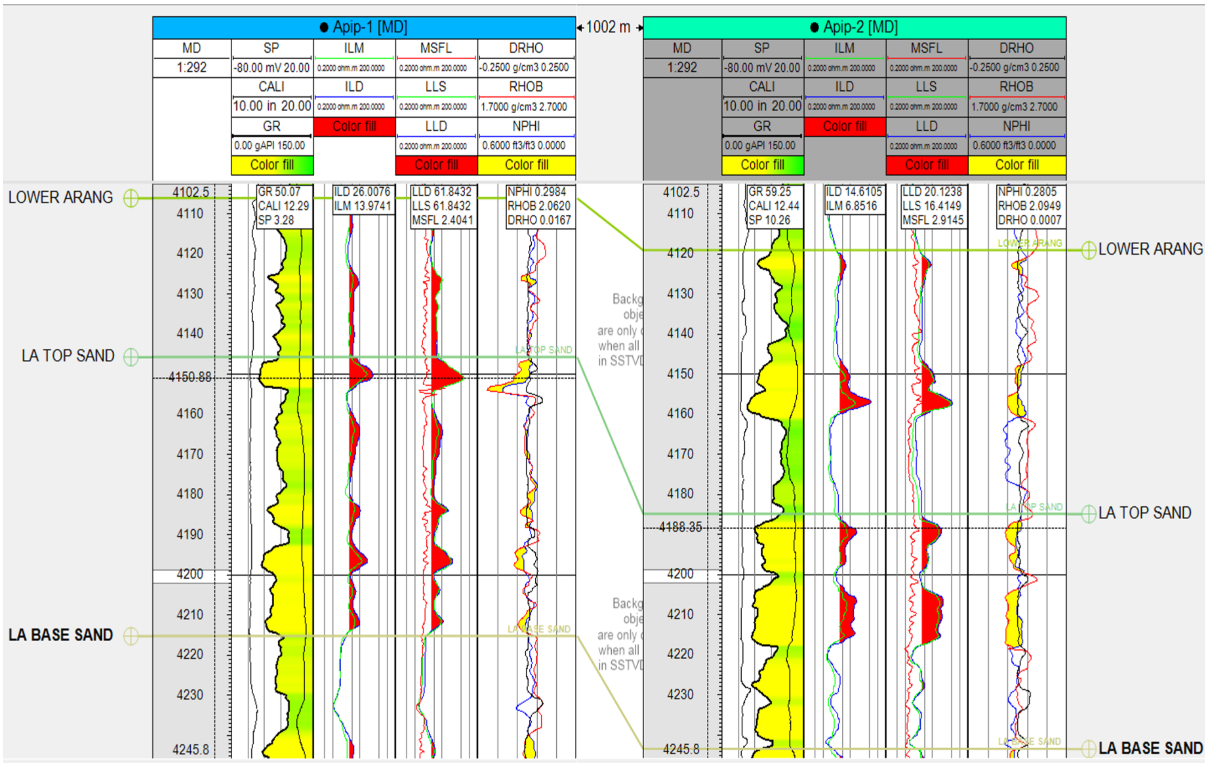

Figure 4. Well log responses (GR, SP, caliper, resistivity, RHOB, NPHI, and DRHO) highlighting the Lower Arang Top Sand interval in Apip-1 and Apip-2, where low GR values, resistivity separation, and RHOB – NPHI responses are used to identify sandstone reservoir intervals and compare reservoir quality between the two wells

Based on the crossplot inflection point between reservoir and non-reservoir cluster at both wells, a reservoir–non-reservoir impedance boundary of approximately 6,200 m/s·g/cc was established as the quantitative cutoff for subsequent polygon delineation (Figures 17 and 18). This threshold is consistent with well-calibrated impedance values separating porous sandstone from tight or shale-dominated intervals (Zahmatkesh et al., 2021).

Time structure map analysis

Time structure map of the Lower Arang Top Sand horizon was generated from 3D seismic interpretation, representing TWT distribution of the target interval (Figure 7). The map showed a structural high developed in the central–northern part of the study area, characterized by relatively shallower TWT values ranging from approximately −1290 to −1320 ms. Toward the southern part, the structure deepened significantly, as indicated by closely spaced contours reflecting steeper structural gradients related to fault-related deformation consistent with the extensional tectonic framework of West Natuna Basin (Doust & Noble 2008).

Overall, both wells are located in the structural high, with Apip-2 positioned along the western flank and Apip-1 situated closer to the structural crest. The relatively closed geometry of the structural culmination indicates an anticline-type structural trap, providing a favorable configuration for hydrocarbon accumulation. In extensional basins like West Natuna, structural highs commonly function as hydrocarbon migration focal points and trap-forming elements (Surjono et al., 2023). This framework establishes the geometric control for reservoir distribution, serving as a critical reference for integrating AI and seismic attribute analysis.

Seismic attribute analysis

Seismic attribute analysis was conducted to evaluate lateral heterogeneity in the Lower Arang Top Sand interval. The selected attributes, including RMS amplitude, variance, envelope, and sweetness, represented reflection energy, structural discontinuity, and qualitative lithological variation. Among these attributes, RMS amplitude is particularly sensitive to AI contrasts and is often used to identify potential sandstone bodies (Chopra & Marfurt 2005). To support quantitative interpretation, amplitude distributions were analyzed by extracting attribute values at Apip-1 and Apip-2 control points and comparing with the spatial distributions observed on horizon maps. These well-calibrated reference values serve as anchor thresholds for identifying reservoir and non-reservoir zones across the 3D volume (Yusuf et al., 2016; Zahmatkesh et al., 2021).

RMS amplitude

RMS amplitude map in Figure 8 shows significant lateral variation in reflection energy across the study area. RMS amplitude values, indicated by red to yellow colors, were predominantly concentrated over the structural high identified in the time structure map, particularly around Apip-2 and partially in Apip-1. This spatial coincidence suggests that the high-energy reflections are structurally controlled and correspond to cleaner sandstone intervals with stronger impedance contrasts relative to surrounding shale units.

Low RMS amplitude zones, indicated by blue to purple colors, dominated the southern, structurally deeper area. These low-energy zones formed elongated patterns consistent with deeper structural trends, which could be interpreted as finer-grained lithologies or shale-dominated intervals.

Amplitude extraction at Apip-1 and Apip-2 showed RMS values of approximately 0.12–0.18 (normalized units) in the identified reservoir interval. Based on the bimodal distributions across the study area, RMS amplitude threshold of approximately 0.10 (normalized) was applied to distinguish high-anomaly zones (potential reservoir) from background (non-reservoir). This threshold corresponds approximately to the mean plus one standard deviation (ì + 1ó) of the background amplitude population, consistent with standard practice for attribute-based reservoir discrimination (Chopra & Marfurt 2007).

Variance attribute

Variance attribute in Figure 9 enhances lateral discontinuities by measuring trace-to-trace

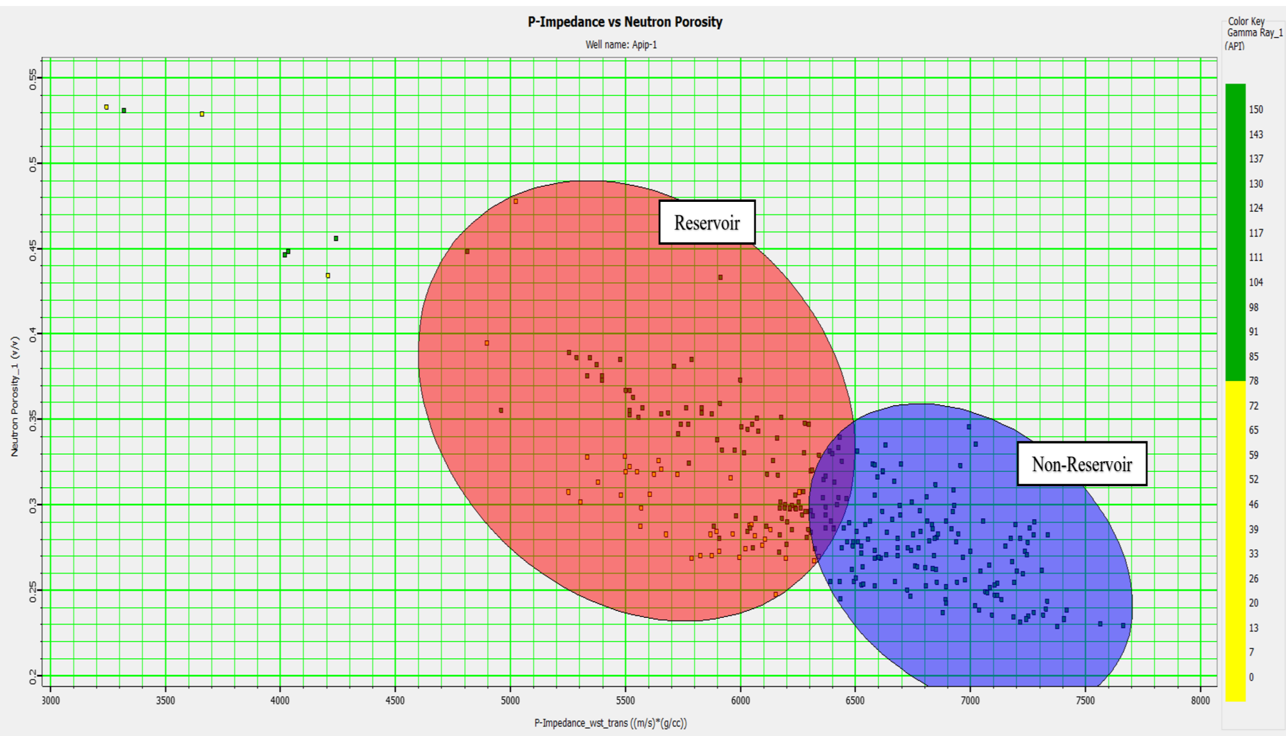

Figure 5. Crossplot of P-impedance versus NPHI for the Lower Arang Top Sand interval in Apip-1, showing an inverse relationship between impedance and porosity, where low P-impedance values of approximately 5,200–6,200 m/s·g/cc and higher NPHI values indicate better sandstone reservoir quality.

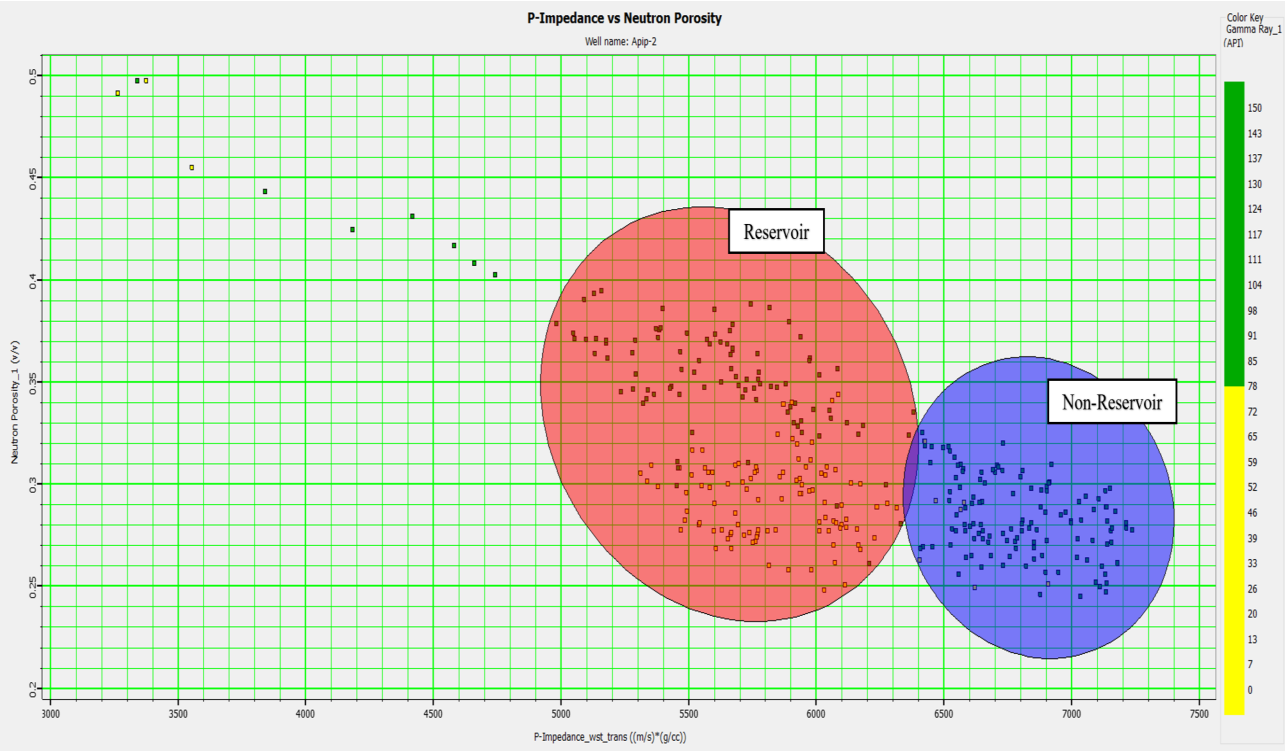

Figure 6. Crossplot of P-impedance versus NPHI for the Lower Arang Top Sand interval in Apip-2, showing a similar inverse impedance – porosity trend, with reservoir intervals characterized by P-impedance values of approximately 5,300–6,200 m/s·g/cc and relatively higher NPHI responses

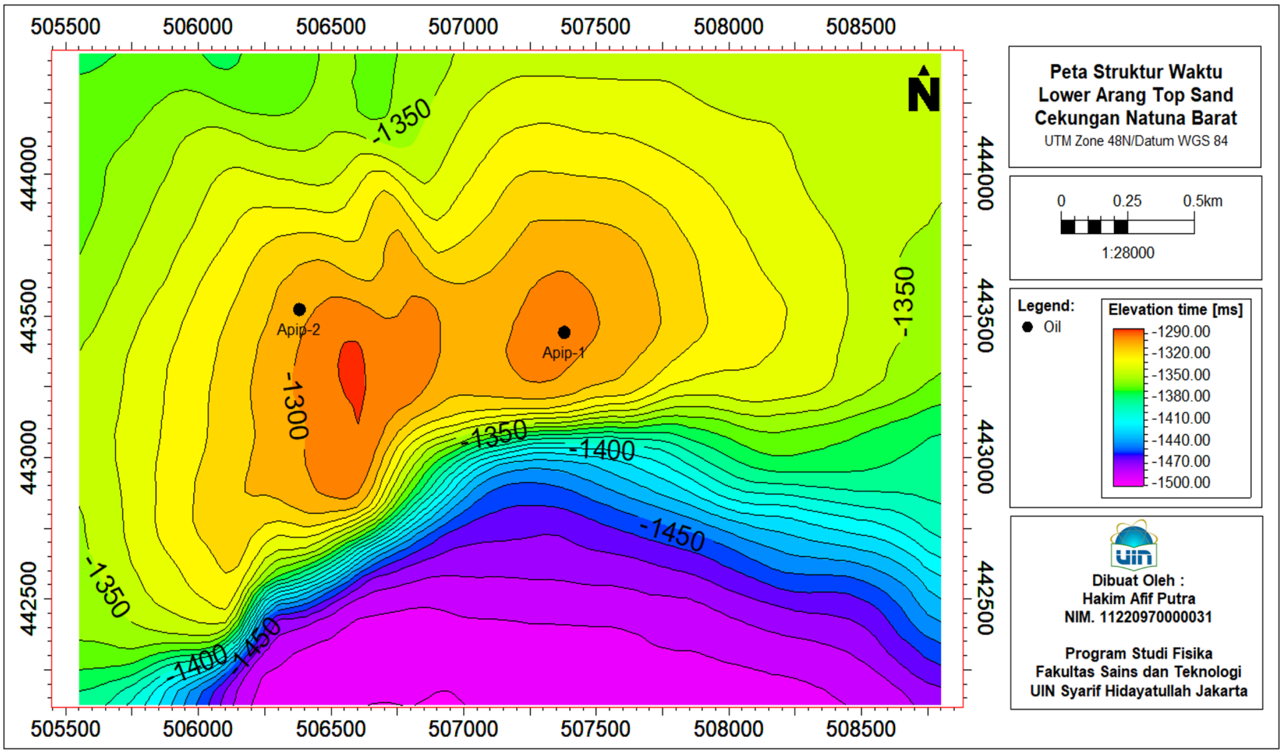

Figure 7. Time structure map of the Lower Arang Top Sand horizon showing structural geometry and the positions of Apip-1 and Apip-2, with shallower TWT values in the central – northern area indicating a structural high that may act as a favorable zone for reservoir development and hydrocarbon accumulation.

waveform variability and is often used to identify faults, fractures, and stratigraphic boundaries (Taner 2001; Chopra & Marfurt 2005). In the study area, elevated variance anomalies were predominantly developed in the southern part, correlating with steep structural gradients observed on the time structure map. This spatial correlation between high variance zones and structural contour tightening suggests fault-related deformation or compartmentalization.

In comparison, central–northern part surrounding the structural high showed relatively low variance values, indicating laterally continuous and stable reflectors. The combined RMS and variance interpretation suggests that reservoir development in the Lower Arang Top Sand is preferentially preserved in structurally coherent zones, while deeper compartments are segmented structurally.

Envelope attribute

Envelope attribute represents the instantaneous amplitude magnitude, showing total seismic energy independent of polarity (Taner et al., 1979). As presented in Figure 10, relatively high envelope values were developed in the central to southern part, forming elongated patterns consistent with the structural trend.

A significant spatial inconsistency was observed between envelope and RMS amplitude distributions. Envelope was highest in the central-to-south part, where the structure was relatively deep and variance values were elevated. Meanwhile, RMS amplitude and sweetness anomalies were concentrated at the northern structural high, indicating differing spatial controls and careful interpretation of these attributes.

Several factors are responsible for the spatial inconsistency observed in the study area. First, depositional controls play a dominant role in the southern part, where isopach thickening of the Lower Arang interval can produce a stronger bulk energy response despite a deeper structural position. This is because thicker sediment accumulations tend to generate higher total envelope values by integrating energy across a

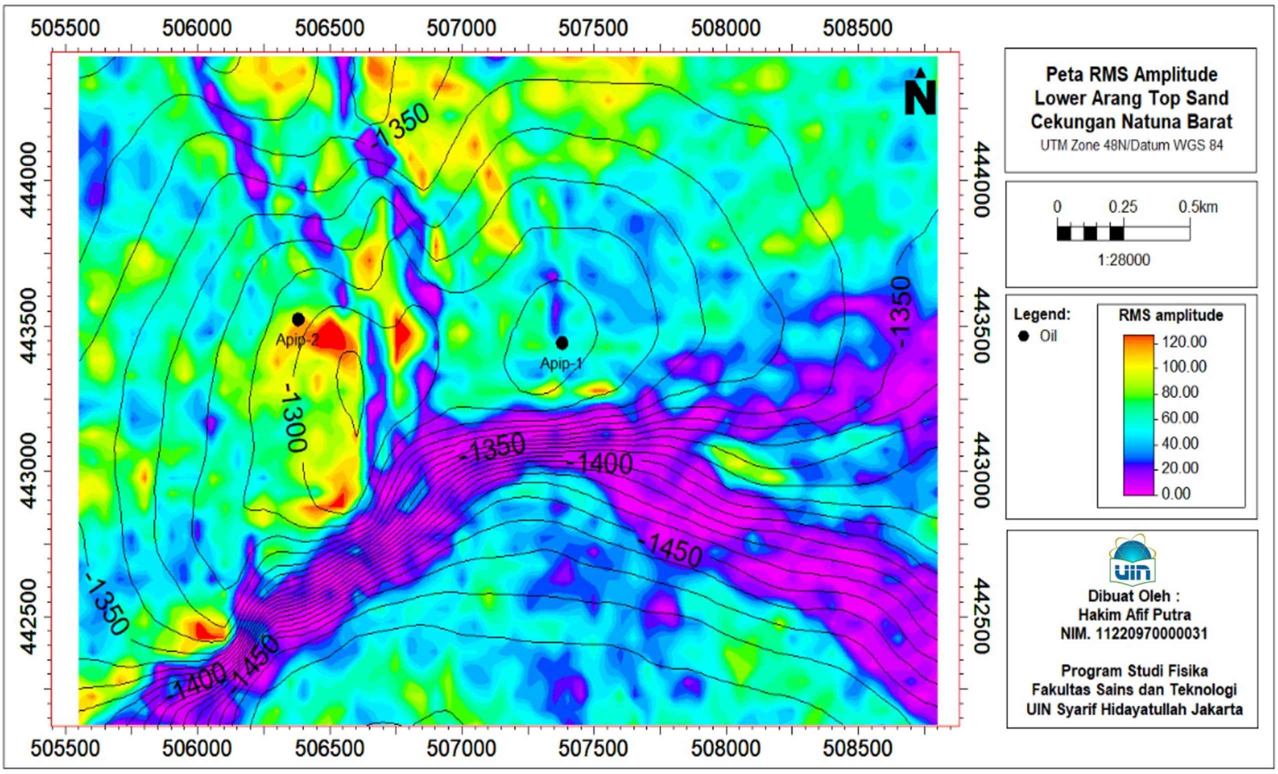

Figure 8. RMS amplitude map of the Lower Arang Top Sand horizon showing lateral variations in seismic reflection energy, where high RMS amplitude anomalies around Apip-2 and part of Apip-1 indicate stronger impedance contrasts associated with potential sandstone reservoir zones, while lower amplitudes in the southern area suggest weaker reservoir response or finer-grained intervals

longer stratigraphic window, even when individual reflectors are weaker. Second, thin-bed tuning effects at the structural crest explain the apparent discrepancy. At the northern structural high, the Lower Arang Top Sand may be near or at the tuning thickness, producing locally strong RMS and high-frequency sweetness responses but relatively lower total envelope energy compared to thicker off-structural equivalents. Third, the polarity independence of envelope attribute makes it more susceptible to coherent noise contributions from structurally complex zones in the south, where higher variance values indicate reflector disruption.

The observations suggest that envelope spatial pattern is primarily controlled by depositional thickness variations and possible tuning interference rather than fluid or lithological content per se. This interpretation is supported by the thickness map (Figure 19), which shows greater TWT thickness in the southern part of the study area. Therefore, envelope distribution provides complementary information about sediment thickness and depositional architecture rather than simply replicating the structural reservoir signal captured by RMS amplitude. This distinction shows the importance of interpreting seismic attributes as an integrated ensemble rather than individually, as each attribute captures different aspects of the subsurface seismic response (Chopra & Marfurt 2007; Taner 2001).

Sweetness attribute

Sweetness attribute is a combination of reflection amplitude and instantaneous frequency. This attribute is often used to show lithological variations associated with porous sandstone bodies (Taner 2001; Chopra & Marfurt 2007). In this study, high sweetness anomalies were predominantly developed in the western to northwestern part, particularly around Apip-2. The observed anomalies spatially coincide with high RMS amplitude zones and the structural high identified on the time structure map, suggesting the presence of relatively clean and porous sandstone bodies in the Lower Arang Top Sand interval.

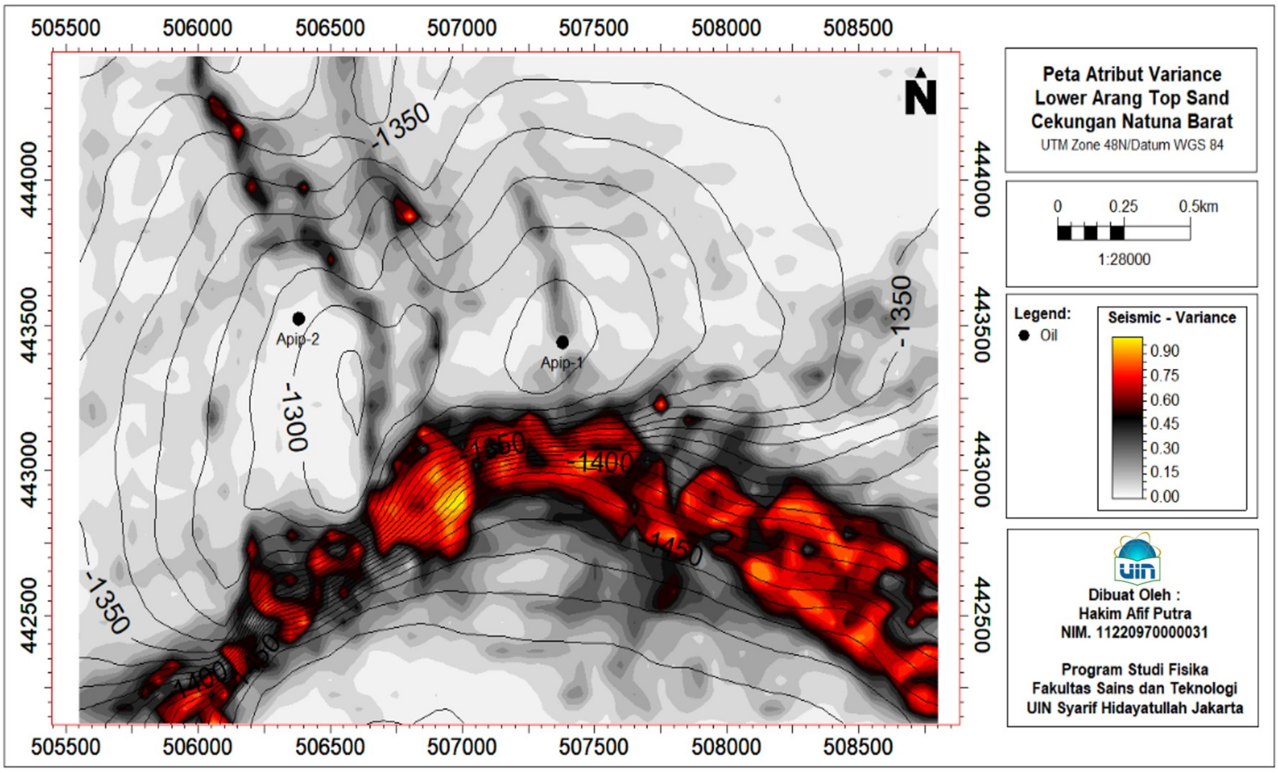

Figure 9. Variance attribute map of the Lower Arang Top Sand horizon showing zones of reflector discontinuity, where higher variance anomalies in the southern area indicate possible fault-related deformation, structural segmentation, or lateral facies changes, while lower variance around the structural high suggests more continuous reflectors.

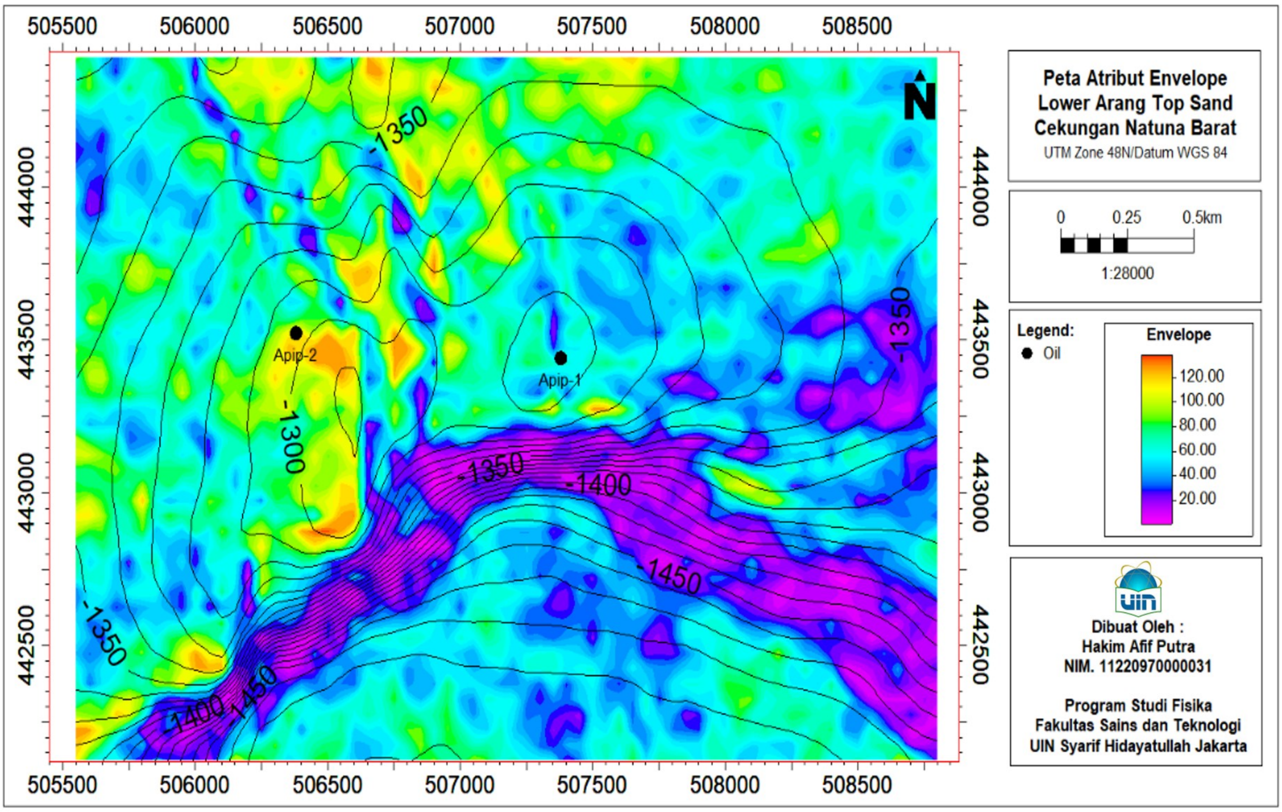

Figure 10. Envelope attribute map of the Lower Arang Top Sand horizon showing the distribution of seismic reflection energy, where variations in envelope response highlight changes in instantaneous amplitude related to depositional thickness, reflector continuity, and possible tuning effects.

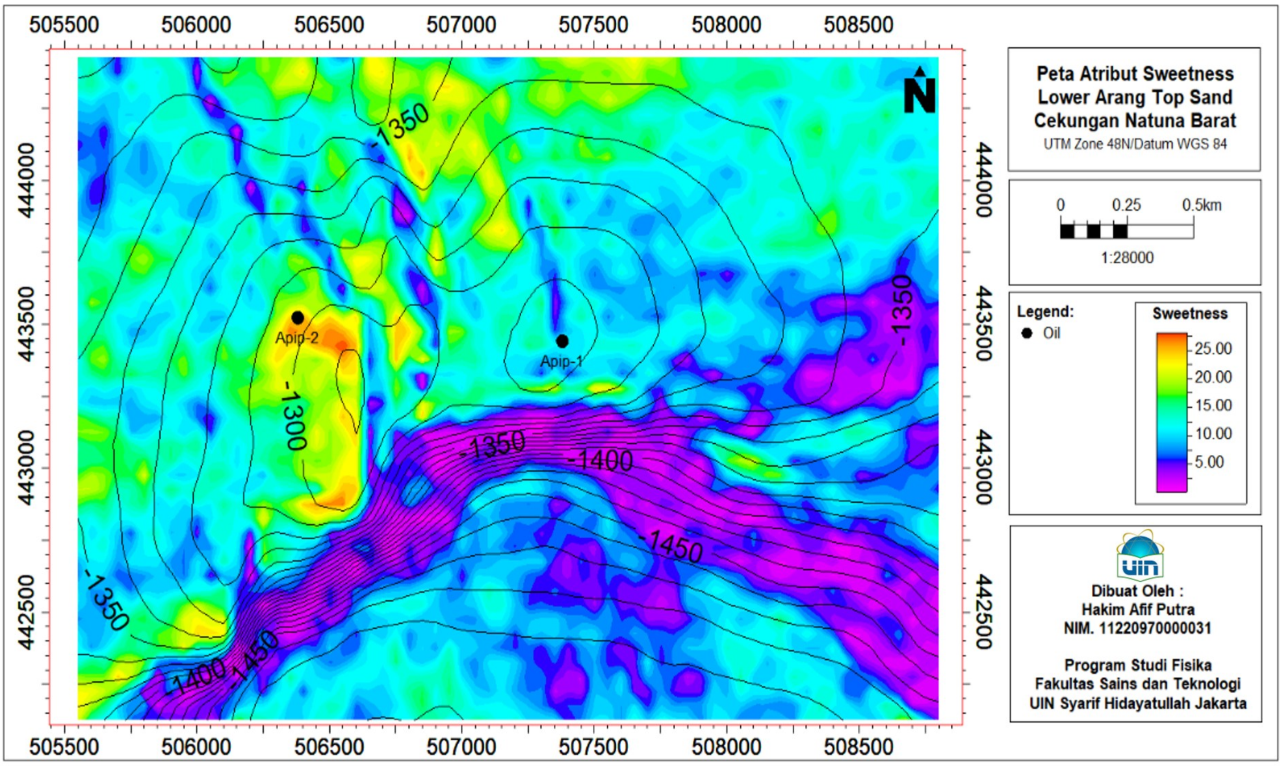

Figure 11. Sweetness attribute map of the Lower Arang Top Sand horizon overlaid with time structure contours and well locations, where higher sweetness anomalies around the western to northwestern structural high near Apip-2 indicate potential porous sandstone development, while lower sweetness values toward the southern area suggest reduced reservoir quality.

Low sweetness values were dominant in the southern and southeastern parts of the study area, corresponding to deeper structural positions and coinciding with zones of elevated variance values. These conditions are interpreted to represent intervals with lower reservoir quality.

The integrated interpretation of RMS amplitude, variance, envelope, and sweetness attributes consistently indicates that the most prospective reservoir zones are concentrated around the structural high, particularly in the vicinity of Apip-2. Meanwhile, the spatial inconsistency of the envelope attribute is attributed to depositional thickness and tuning effects. The convergence of multiple attribute anomalies at Apip-2 structural high provides stronger confidence in the reservoir interpretation compared to any single attribute in isolation.

Initial acoustic impedance model

Initial P-impedance model was constructed by integrating seismic data, well log-derived impedance from Apip-1 and Apip-2, and interpreted stratigraphic horizons. The model serves as a low-frequency constraint in the model-based inversion process, providing the background impedance trend necessary for stabilizing inversion results.

Figure 12 shows initial impedance model along an arbitrary seismic line intersecting both wells. In the Lower Arang Top Sand interval, P-impedance values range from approximately 5,200 to 6,200 m/s·g/cc. This is consistent with the presence of sandstone units with moderate to good porosity, as indicated by well log analysis and crossplot results. Therefore, this initial impedance framework provides a reliable starting condition for the further AI inversion process.

Acoustic impedance iversion results

Model-based AI inversion was carried out using a zero-phase statistical wavelet constrained by the interpreted horizons and the initial impedance model. Inversion quality was evaluated through well-to-seismic comparison by examining correlation coefficient (CC) and error values between synthetic and observed seismic traces at the well locations.

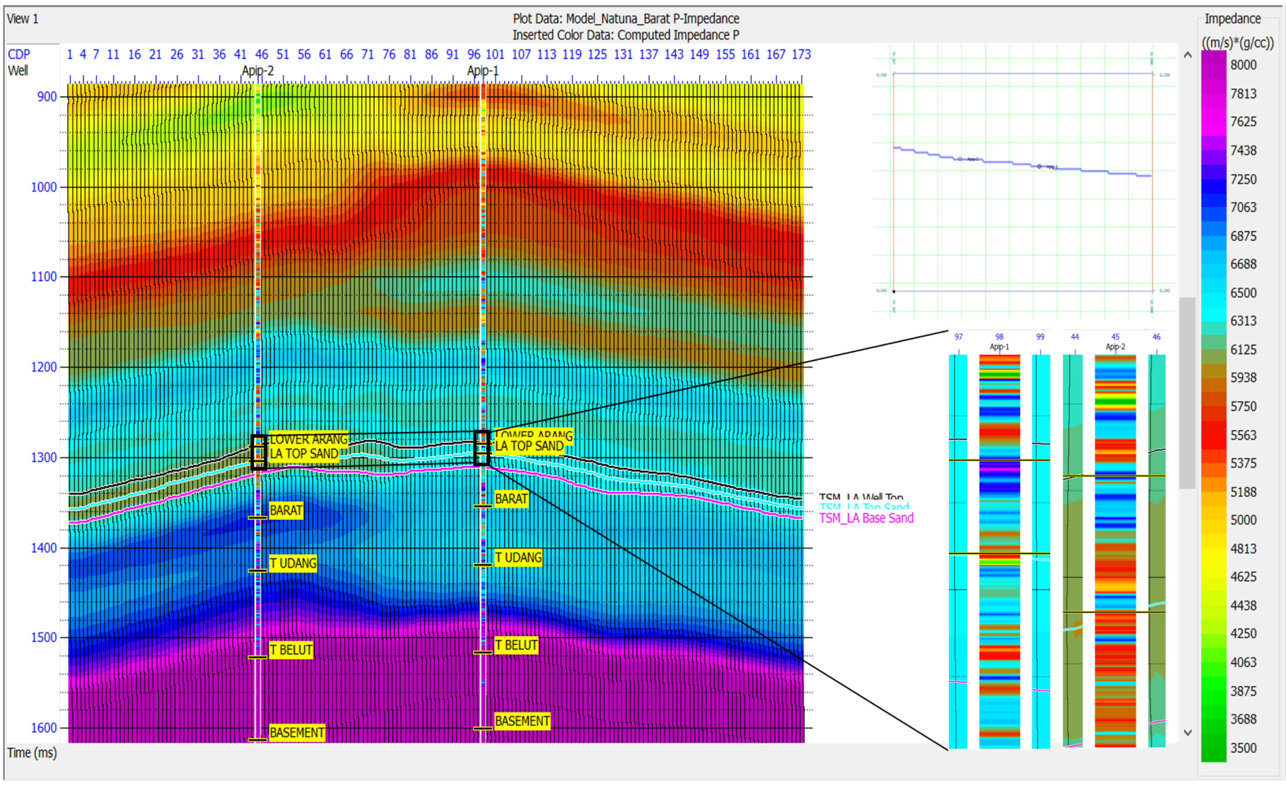

Figure 12. Initial P-impedance model along an arbitrary seismic line intersecting Apip-1 and Apip-2, showing the initial impedance distribution of the Lower Arang Top Sand interval, with values of approximately 5,200–6,200 m/s稳/cc used

At Apip-1, the inversion result obtained a CC of approximately 0.987 with an error value of 0.16, indicating an excellent match between the synthetic seismogram and the real seismic trace. Similarly, Apip-2 showed CC of approximately 0.981 with an error of 0.19, indicating a high level of consistency.

The substantially higher CC values obtained from the inversion result (~0.987 and ~0.981) relative to the initial well–seismic tie (~0.93 and ~0.97) show the iterative nature of the model-based inversion process. Therefore, these CC should not be interpreted as independent validation of the inversion. In model-based inversion, the algorithm iteratively updates the impedance model to minimize the least-squares misfit between synthetic and observed seismic traces. Since the low-frequency model is directly derived from and constrained by well log impedance at both Apip-1 and Apip-2, the inversion inherently converges toward solutions that closely reproduce the seismic response at well locations. The process is fundamentally different from the initial well–seismic tie, which evaluates wavelet extraction accuracy without model updating. This shows that the higher CC values achieved after inversion mainly indicate improved numerical convergence between the modeled and observed seismic responses at the well control points, rather than reflecting predictive accuracy in the entire 3D seismic volume.

The inversion is constrained by only two wells in a 3D volume, introducing a non-negligible risk of bias toward the initial impedance model. Consequently, the high CC values at well points should be interpreted as indicators of numerical consistency and inversion stability at the constrained positions, rather than as measures of prediction accuracy in inter-well zones. The inverted impedance volume provides reliable interpretations, where the model is well-constrained by well data, while inter-well zones require integration with seismic attribute analysis as complementary evidence (Hampson et al., 2005).

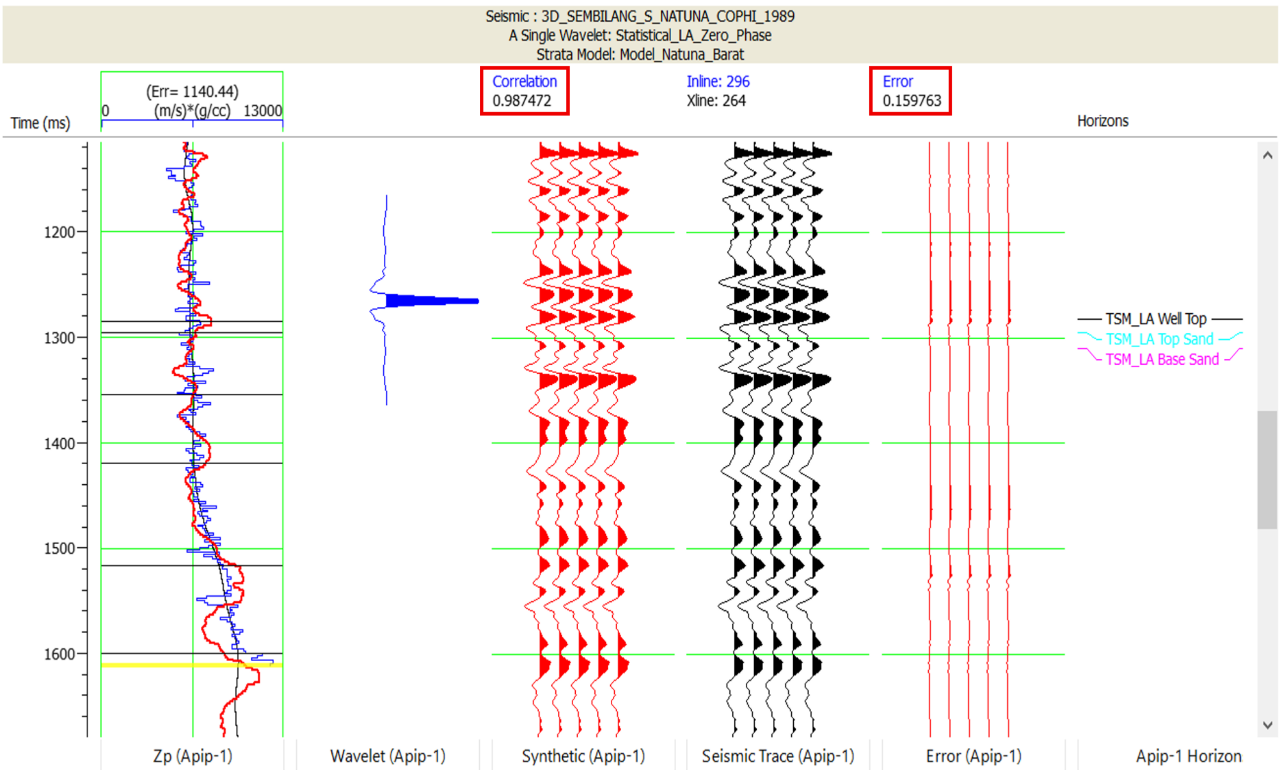

Figure 13. Model-based AI inversion result at Apip-1 showing high correlation and low error, with a correlation coefficient of approximately 0.987 and an error value of 0.16, indicating good numerical consistency between the synthetic and observed seismic traces at the well location

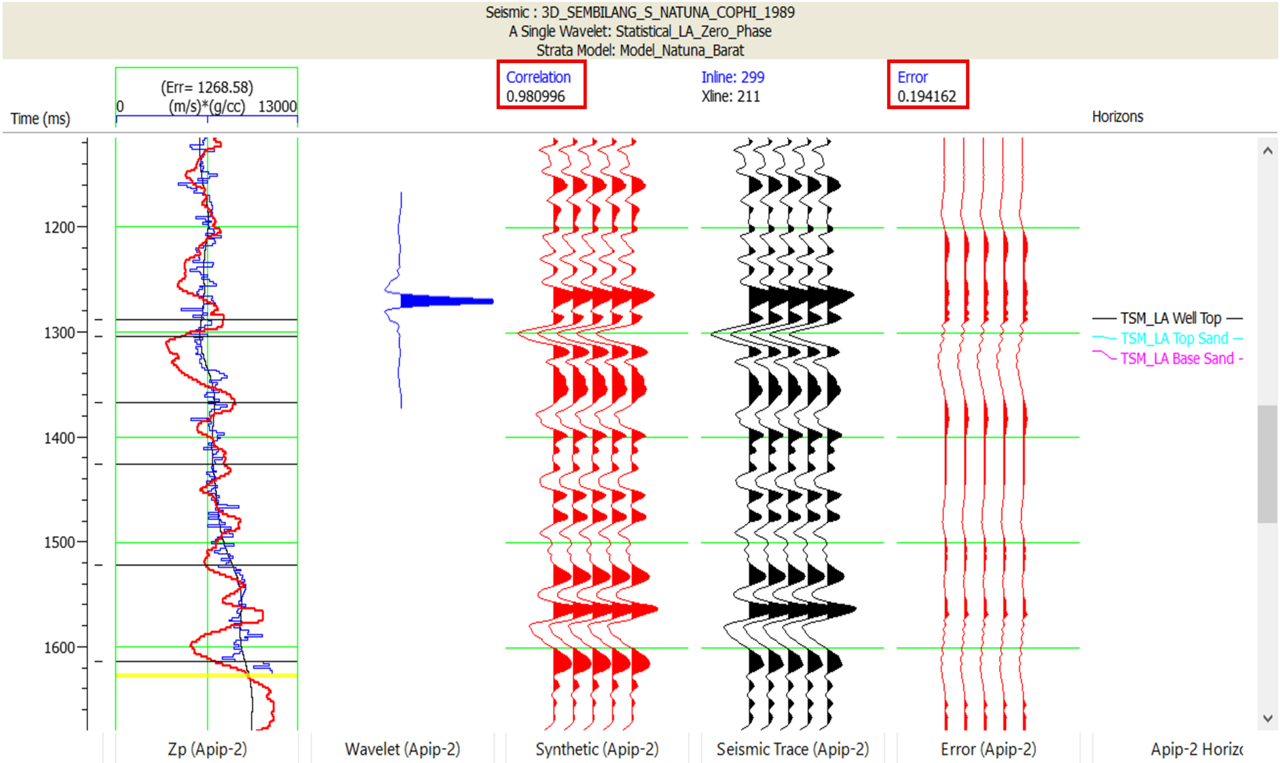

Figure 14. Model-based AI inversion result at Apip-2 showing good agreement between inverted and well log impedance, with a correlation coefficient of approximately 0.981 and an error value of 0.19, indicating stable inversion results at the well control point.

Acoustic impedance section and horizon extraction

The inverted AI section along the arbitrary seismic line intersecting Apip-1 and Apip-2 showed laterally continuous impedance variations in the Lower Arang Top Sand interval (Figure 15). Relatively low impedance zones were also observed around the structural high near Apip-2 and extend laterally toward the central part of the study area. These zones correspond with reservoir interval identified from well log analysis and crossplot interpretation.

In comparison, impedance values progressively increased toward the southern part, as the structure deepened. This is interpreted to show compaction effects or increased shale content, reducing reservoir quality compared to the structurally elevated zones.

AI values extracted along the Lower Arang Top Sand horizon in Figure 16 showed distinct lateral heterogeneity. The results indicate that relatively low impedance zones are concentrated around the western to northwestern part of the structure, particularly near Apip-2, showing potential sandstone reservoirs with better porosity. Higher impedance values dominated the southern and southeastern parts, corresponding to deeper structural positions and coinciding with low RMS amplitude and higher variance responses. Moreover, the consistency between well log responses, crossplot analysis, seismic attributes, and AI inversion results shows that the most prospective reservoir zones are concentrated around the structural high, particularly in the vicinity of Apip-2.

Reservoir geometry: polygon axis and margin

Reservoir geometry was interpreted through polygon axis and margin delineation by integrating RMS amplitude and AI maps of the Lower Arang Top Sand horizon. Zones characterized by consistently high RMS amplitude and relatively low AI were interpreted as the reservoir axis, showing stronger impedance contrast and potentially better sandstone development.

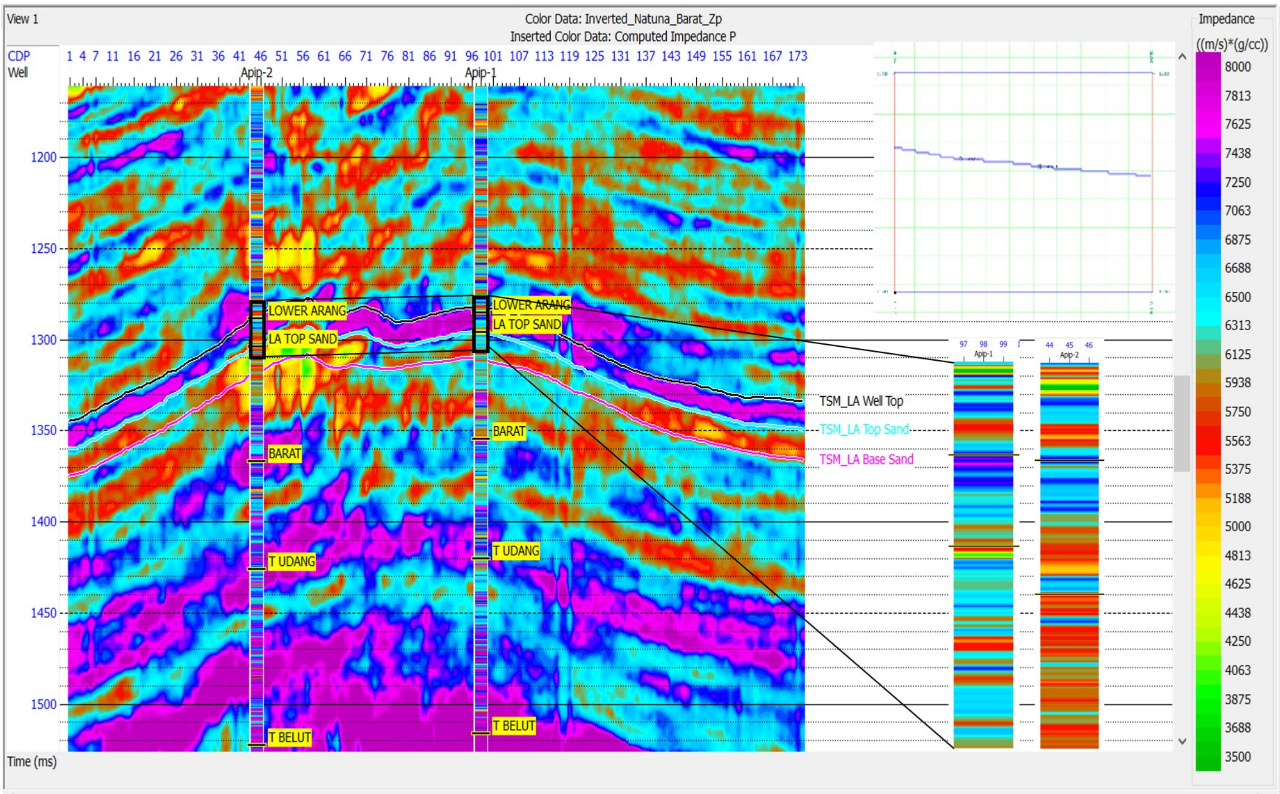

Figure 15. AI inversion section along an arbitrary line intersecting Apip-1 and Apip-2, showing lateral impedance variations in the Lower Arang Top Sand interval, where relatively low AI zones around the structural high near Apip-2 indicate potential porous sandstone reservoir development

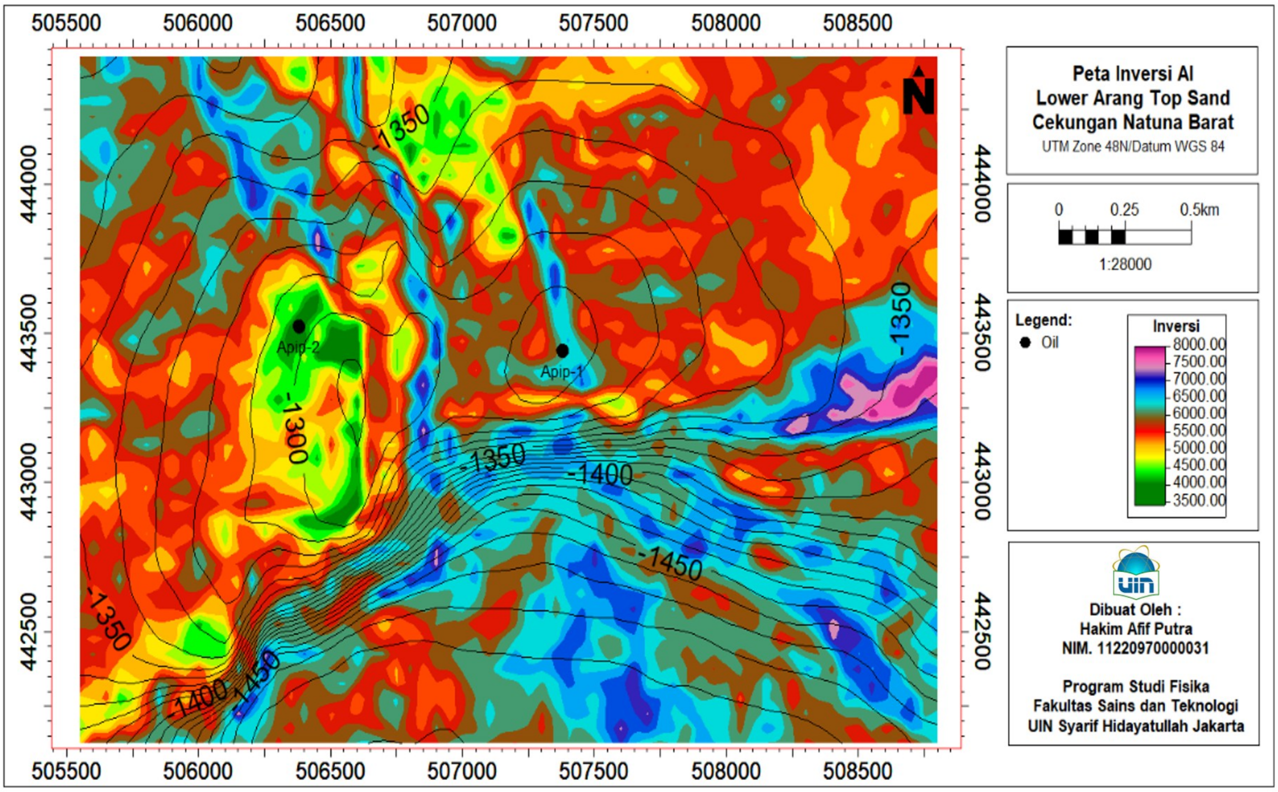

Figure 16. AI extraction map at the Lower Arang Top Sand horizon showing lateral impedance distribution, where relatively low AI zones around the western to northwestern structural high near Apip-2 indicate potential porous sandstone reservoir development, while higher AI values toward the southern and southeastern areas suggest tighter or lower-quality intervals.

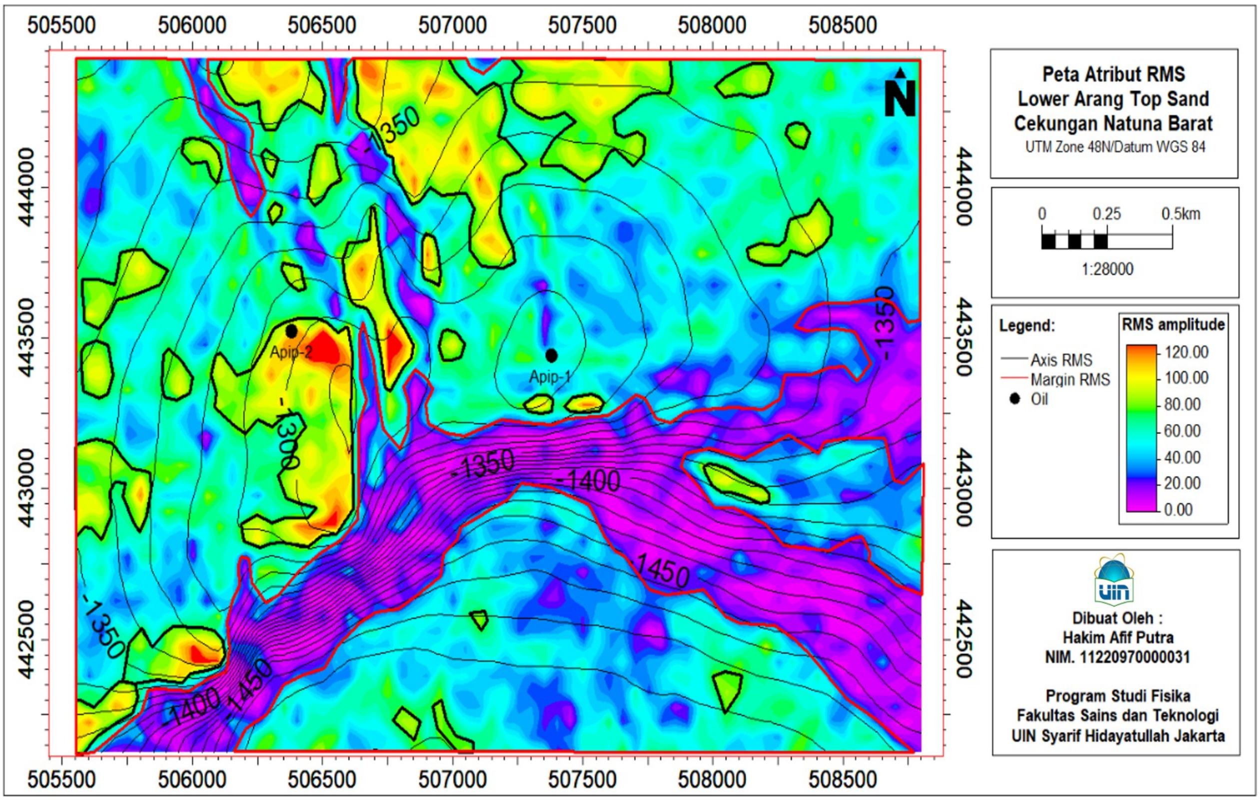

Figure 17. RMS amplitude map with interpreted reservoir axis and margin polygons at the Lower Arang Top Sand horizon, showing that the reservoir axis is associated with higher RMS amplitude anomalies, while the margin zones are characterized by weaker amplitude responses.

Meanwhile, those with lower amplitude responses and higher impedance values were interpreted as reservoir margin zones.

The reservoir–non-reservoir impedance boundary of approximately 6,200 m/s·g/cc (established from crossplot analysis, as discussed in Section 3.2) was applied to guide polygon delineation. This ensured that interpreted boundaries were grounded in quantitative petrophysical data rather than visual estimation. Attribute distribution analysis at Apip-1 and Apip-2 control points further confirmed that zones in the delineated reservoir polygons were associated with below-threshold AI values and above-threshold RMS amplitude responses (Zahmatkesh et al., 2021; Yusuf et al., 2016).

The interpreted reservoir axis forms elongated trends generally following the dominant structural orientation of the study area. The most prominent axis development occurs in the western to northwestern part around Apip-2, where strong RMS amplitude anomalies coincide with low AI values. This spatial correlation indicates the presence of relatively clean sandstone bodies with better reservoir quality. In comparison, the reservoir axis near Apip-1 appears narrower and more fragmented, potentially showing lateral facies variation, localized compaction, or reduced sandstone thickness. The southeastern part is dominated by reservoir margin zones characterized by higher impedance and weaker amplitude responses.

Thickness and overlay analysis

Thickness map of the Lower Arang Top Sand interval in Figure 19 shows lateral variations ranging from approximately 10 to 25 ms TWT. Specifically, values of 10–20 ms TWT dominate the central part around Apip-1 and Apip-2, indicating moderately thick and laterally continuous sandstone development. Localized thicker zones are observed toward the southwestern part of the map, suggesting possible depositional thickening along structural or stratigraphic trends. This thickening pattern in the south is consistent with the higher envelope values, indicating that depositional controls drive envelope spatial pattern rather than reservoir quality variations.

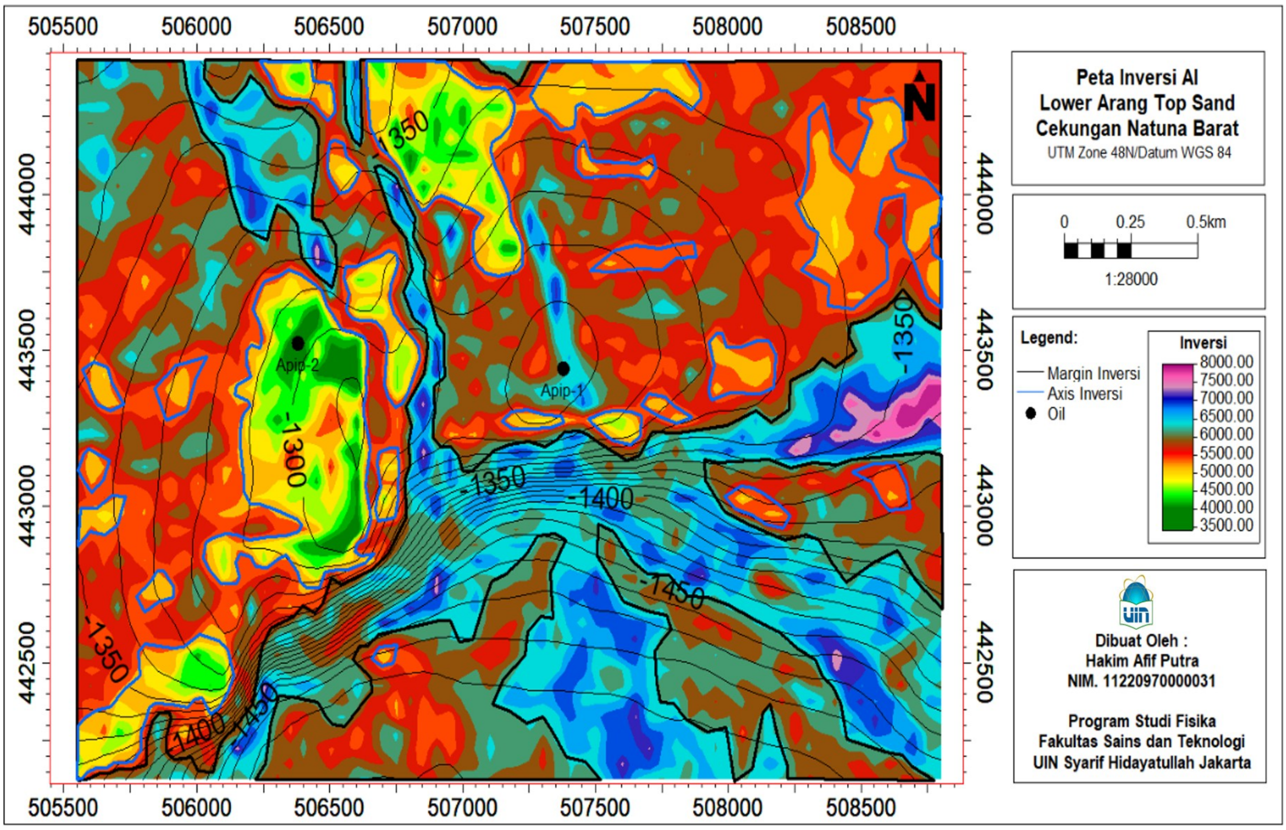

Figure 18. AI map highlighting impedance contrasts between reservoir axis (AI < ~6,200 m/s·g/cc) and margin zones, where low-impedance polygons represent potential porous sandstone reservoir bodies and higher-impedance areas indicate tighter or non-reservoir intervals.

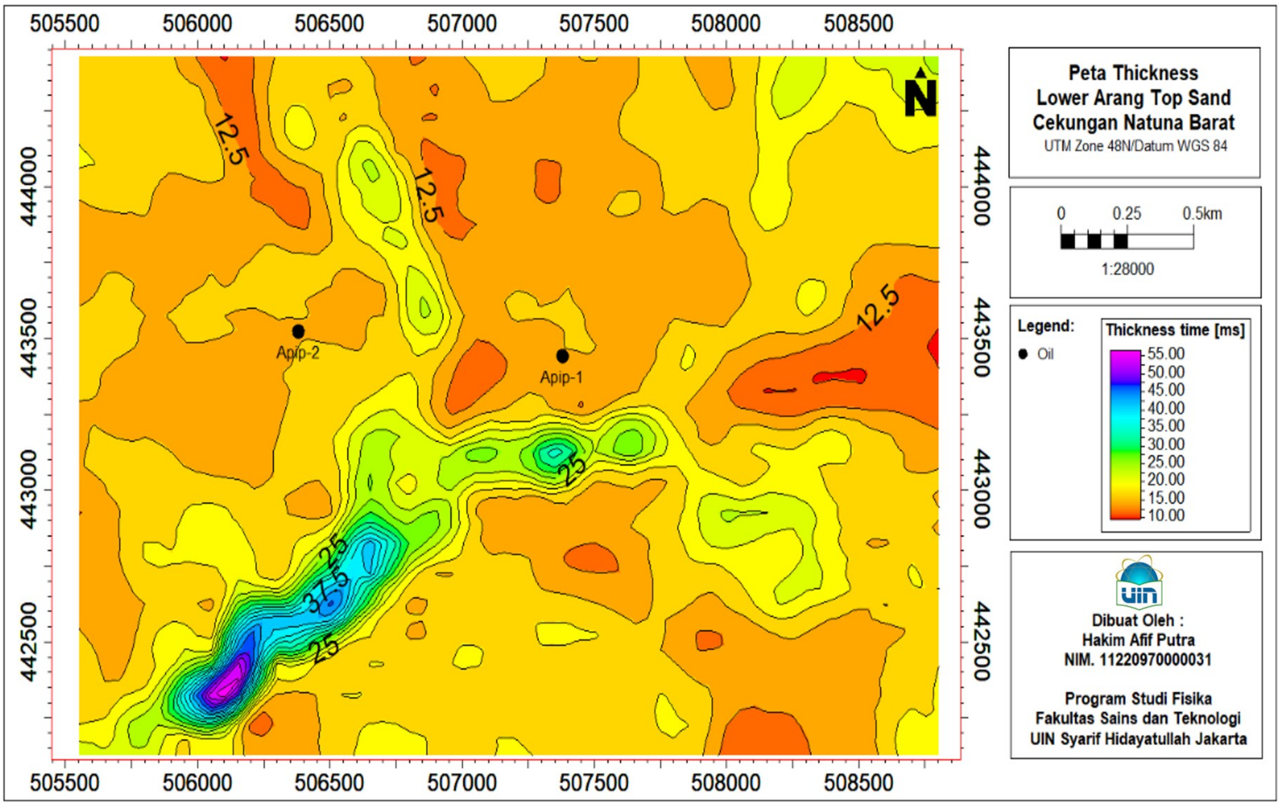

Figure 19. Thickness map of the Lower Arang Top Sand interval showing thickness distribution in ms TWT, where moderate thickness around Apip-1 and Apip-2 indicates laterally continuous sandstone development, while localized thickening toward the southwestern area suggests depositional thickening along structural or stratigraphic trends

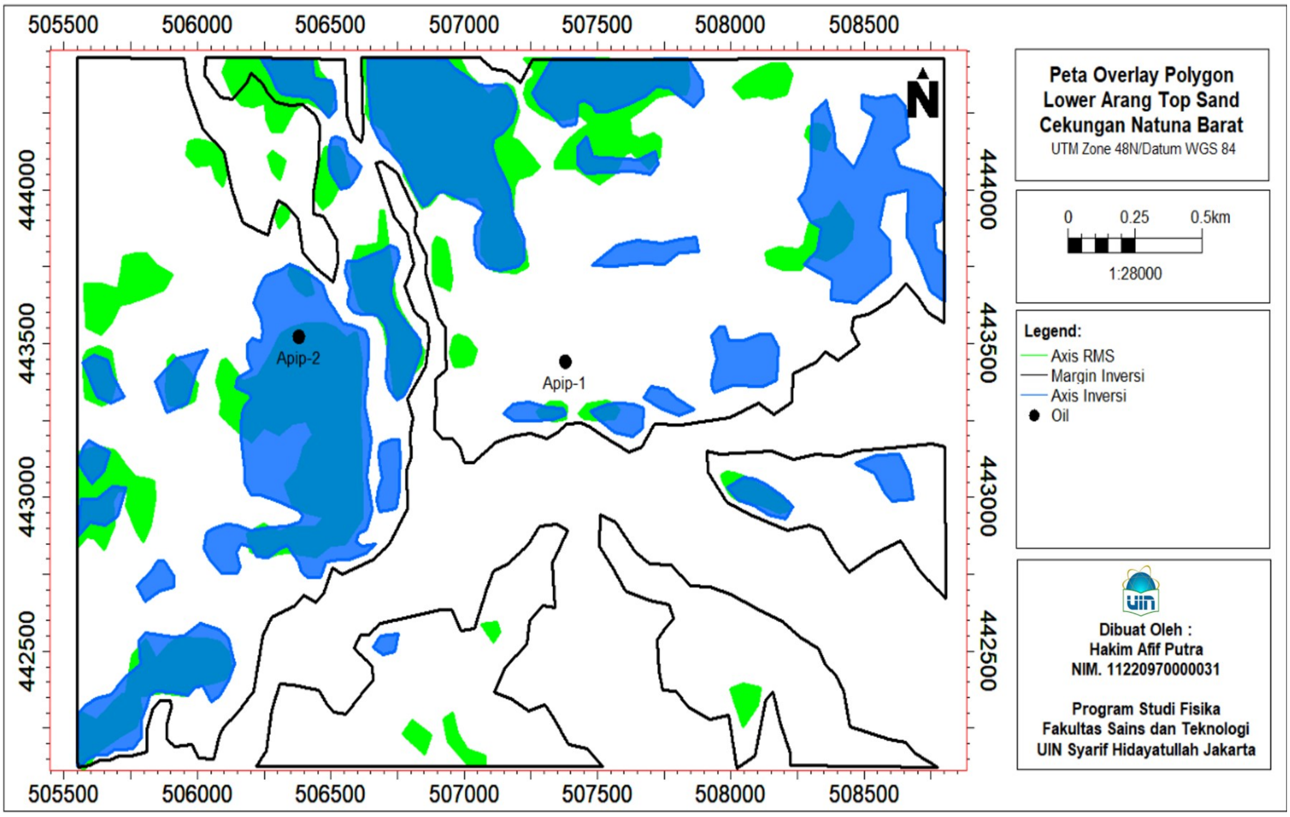

Figure 20. Overlay map integrating RMS amplitude, AI polygons, thickness distribution, and well locations, showing the coincidence of favorable reservoir indicators around Apip-2, where high RMS response, low AI reservoir axis, and moderate thickness support better lateral reservoir continuity.

An overlay analysis integrating RMS amplitude anomalies, AI polygons, thickness distribution, and well in Figure 20 shows zones where favorable reservoir indicators coincide. The overlay results indicate that the most laterally continuous and prospective reservoir zones are concentrated around Apip-2, where attribute anomalies and impedance-derived reservoir axes coincide with moderate sandstone thickness. In comparison, the reservoir distribution near Apip-1 appears thinner and more fragmented.

CONCLUSION

In conclusion, this study shows that reservoir characteristics of the Lower Arang Formation in West Natuna Basin can be effectively determined by integrating well log analysis, seismic attributes, and AI inversion. The results show that well log responses in the Lower Arang Top Sand interval indicate sandstone lithology characterized by relatively low GR values, moderate to good porosity, and higher resistivity compared to surrounding non-reservoir intervals.

Crossplot analysis between P-impedance and NPHI confirms an inverse relationship between AI and porosity, establishing a quantitative reservoir-non-reservoir boundary at approximately 6,200 m/s·g/cc. This threshold is applied to guide reservoir polygon delineation, providing a data-driven rather than qualitative basis for reservoir geometry interpretation.

Petrophysical analysis using Archie's equation shows comparable fluid saturation conditions between the two wells. Estimated Sw values at Apip-1 (approximately 0.35–0.50) suggest a transitional interval with hydrocarbon indication, while Apip-2 (approximately 0.40–0.50) indicates a similar transitional zone. The resistivity contrast between the two wells is attributed to local compaction or salinity differences.

Seismic attribute analysis shows that high RMS amplitude and sweetness anomalies are spatially associated with low AI zones and structural highs. This indicates that reservoir development in the Lower Arang Top Sand interval is influenced by both structural configuration and depositional architecture. Furthermore, the spatial inconsistency of envelope attribute relative to RMS and sweetness shows depositional thickness variations and thin-bed tuning effects rather than reservoir quality differences, indicating the importance of integrated multi-attribute interpretation.

The high correlation coefficient values of approximately 0.987–0.981 obtained from model-based AI inversion show numerical convergence of the constrained model at the control points and should be interpreted in the context of only two well controls. These values do not imply equivalent accuracy in inter-well zones, where seismic attribute integration provides complementary constraints.

The integrated interpretation of AI inversion, seismic attributes, petrophysical analysis, and thickness distribution indicates the distribution of reservoir quality across the study area. The most prospective reservoir zones are concentrated around Apip-2, where sandstone bodies show better lateral continuity and more favorable hydrocarbon indicators. Overall, the applied workflow provides an effective and quantitatively grounded approach for delineating reservoir distribution in similar clastic reservoir systems within the West Natuna Basin.

ACKNOWLEDGEMENT

The authors are grateful to the Department of Physics, Faculty of Science and Technology, Syarif Hidayatullah State Islamic University Jakarta, for the academic support provided during this study. The authors also would like to thank PT Patra Nusa Data and the Ministry of Energy and Mineral Resources of the Republic of Indonesia (ESDM) for supporting the availability of seismic and well log data used in this study. Furthermore, the authors sincerely acknowledge the reviewers, editorial team, and committee of Scientific Contributions Oil and Gas (SCOG) LEMIGAS for their valuable comments, constructive suggestions, and support during the publication process.

DECLARATIONS

Author contribution

Author Contributions: Hakim Afif Putra (conceptualization, data processing, seismic attribute analysis, acoustic impedance inversion, reservoir interpretation, visualization, writing – original draft, writing – review and editing, manuscript revision); Edi Sanjaya (project administration, funding acquisition, publication support, data quality control, supervision); Suwondo (supervision, conceptual validation, methodology validation, theoretical guidance, data interpretation validation, post-review revision validation); Muhammad Nafian (project administration, funding acquisition, publication support, supervision); Praditiyo Riyadi (geophysical review, seismic interpretation validation, structural interpretation validation, post-review revision validation); Widi Atmoko (resources, data support, geological review, well log analysis, petrophysical interpretation, data validation). All authors have read and agreed to the published version of the manuscript.

Funding statement

The authors declare that this research received no specific external funding. Institutional support was limited to academic supervision, publication support, and data access facilitation.

Competing interest

The authors declare that they have no known competing financial interests or personal relationships that could have influenced the work reported in this paper.

The use of AI or AI-assisted technologies

The authors used AI-assisted tools only to support language editing, grammar checking, and manuscript formatting. After using these tools, the authors reviewed and edited the content as needed and take full responsibility for the scientific content, interpretation, and conclusions of the manuscript.

GLOSSARY OF TERMS AND SYMBOLS

Terms & Symbols	Definition	Unit
AI	Acoustic impedance	m/s·g/cc
TWT	Two-way travel time	ms
GR	Gamma ray	API
SP	Spontaneous potential	mV
RHOB	Bulk density	g/cm³
NPHI	Neutron porosity	v/v
ILD	Deep induction resistivity	ohm·m
LLD	Deep laterolog resistivity	ohm·m
LLS	Shallow laterolog resistivity	ohm·m
MSFL	Micro-spherically focused log	ohm·m
DRHO	Density correction	g/cm³
RMS	Root Mean Square (amplitude)	—
Vp	P-wave velocity	m/s
ρ	Bulk density	g/cm³
Sw	Water saturation	fraction
Rw	Formation water resistivity	ohm·m
Rt	True formation resistivity	ohm·m
φ	Effective porosity	fraction or v/v
a	Archie tortuosity factor	—
m	Archie cementation exponent	—
n	Archie saturation exponent	—
Vsh	Shale volume	fraction
CC	Correlation Coefficient	—

REFERENCES

Aki, K. & Richards, P.G., (2002), Quantitative Seismology, 2nd ed. University Science Books.

Antariksa, G., Mukerji, T. & Murti, N.R., (2023), Deep sequence model-based approach to well log data imputation and petrophysical analysis: A case study on the West Natuna Basin, Indonesia. Journal of Applied Geophysics, 218, 105213. https://doi.org/10.1016/j.jappgeo.2023.105213.

Archie, G.E., (1942), The electrical resistivity log as an aid in determining some reservoir characteristics. Transactions of the AIME, 146 (1), pp.54–62.

Asquith, G. & Krygowski, D., (2004), Basic Well Log Analysis, 2nd ed. American Association of Petroleum Geologists (AAPG).

Castagna, J.P., (2003), Petrophysical imaging using seismic inversion. The Leading Edge, 22(2), pp.128–133.

Chopra, S. & Marfurt, K.J., (2005), Seismic attributes—A historical perspective. Geophysics, 70(5), pp.3SO–28SO.

Chopra, S. & Marfurt, K.J., (2007), Seismic Attributes for Prospect Identification and Reservoir Characterization. Society of Exploration Geophysicists.

Doust, H. & Noble, R.A., (2008), Petroleum systems of Indonesia. Marine and Petroleum Geology, 25(2), pp.103–129.

Hampson, D., Russell, B. & Bankhead, B., (2005), Simultaneous inversion of pre-stack seismic data. SEG Expanded Abstracts, 24(1), pp.1633–1637.

Haris, A. et al., (2021), Performance evaluation of machine learning-based classification with rock-physics analysis of geological lithofacies in Tarakan Basin, Indonesia. Journal of Petroleum Science and Engineering, 200, 109250. https://doi.org/10.1016/j.petrol.2021.109250.

Latimer, R., Davison, R. & van Riel, P., (2000), An interpreter's guide to seismic-derived acoustic impedance. The Leading Edge, 19(3), pp.290–297.

Mavko, G., Mukerji, T., & Dvorkin, J., (1998), The Rock Physics Handbook: Tools for Seismic Analysis in Porous Media. Cambridge University Press.

Paskah, L.A. et al., (2018), Fasies pengendapan batupasir Formasi Arang bagian tengah di Lapangan LP, Cekungan Natuna Barat. Padjadjaran Geoscience Journal.

Rachmad, A.A., Djuhaeni, D. & Sumintadiredja, P., (2017), Tektonostratigrafi dan sikuen stratigrafi endapan Lisu Blok Duyung, Cekungan Natuna Barat. Bulletin of Geology ITB.

Rider, M.H. & Kennedy, M., (2011), The Geological Interpretation of Well Logs, 3rd ed. Whittles Publishing.

Schlumberger, (1989), Log Interpretation Principles/Applications. Schlumberger.

Sheriff, R.E. & Geldart, L.P., (1995), Exploration Seismology, 2nd ed. Cambridge University Press.

Surjono, S.S. et al., (2023), Sedimentology and reservoir characteristics of syn-rift to syn-inversion succession in Anoa half-graben, West Natuna Basin, Indonesia. Marine and Petroleum Geology, 152, 106248.

Taner, M.T., (2001), Seismic attributes. CSEG Recorder.

Taner, M.T., Koehler, F. & Sheriff, R.E., (1979), Complex seismic trace analysis. Geophysics, 44 (6), pp.1041–1063.

Verma, S. & Bhattacharya, S., (2025), XAI-driven contamination for self-supervised denoising with pixel-level anomaly detection in seismic data. Journal of Applied Geophysics, 231, 105723. https://doi.org/10.1016/j.jappgeo.2025.105723.

Yusuf, M., Permadi, P., & Rachmat, S., (2016), Analisis porositas dan saturasi air dalam integrasi petrophysics dan seismic multiattributes untuk karakterisasi reservoir. Berkala Fisika, Universitas Diponegoro. https://ejournal3.undip.ac.id/index.php/bfd/article/view/14091.

Zahmatkesh, I. et al., (2021), Integration of well log-derived facies and 3D seismic attributes for reservoir characterization. Journal of Petroleum Science and Engineering, 202, 108442.

Mawalid, A., Haris, A. & Wijanarko, E., (2026), Enhancing Subsurface Geological Model Resolution in Challenging Seismic Conditions by Using Model-Based Deterministic Inversion. *Scientific Contributions Oil and Gas (SCOG)*, 49(1), pp. 121–134. https://doi.org/10.29017/scog.v49i1.1976.

Syahputra, G.A., Haris, A., Wibowo, R.A., & Wijanarko, E., (2026), Reservoir Characterization of the Terumbu and Arang Formations Using Model-Based Seismic Inversion in the East Natuna Basin. *Scientific Contributions Oil and Gas (SCOG)*, 49(1), pp. 135–150. https://doi.org/10.29017/scog.v49i1.1979.

Haris, A., Haryono, H. and Riyanto, A., (2018), Spectral decomposition technique based on STFT and CWT for identifying the hydrocarbon reservoir. *Scientific Contributions Oil and Gas*, 40(3), pp. 125–131. https://doi.org/10.29017/SCOG.40.3.50.

Butar, M.H.P.B., Juventa and Marlinda, L., (2023), Identifikasi prospek reservoir hidrokarbon menggunakan inversi impedansi akustik pada Blok Kampar. *Lembaran Publikasi Minyak dan Gas Bumi*, 57(1), pp. 43–59. https://doi.org/10.29017/LPMGB.57.1.1324.

Taqiy, Z.F., Utomo, W., Shidqii, M. & Susilo, A., (2025), Karakterisasi Reservoar Berdasarkan Analisis Inversi Seismik Impedansi Akustik dan Multiatribut Seismik, Studi Kasus: Lapangan Bunyu Tapa, Cekungan Tarakan, Kalimantan Utara. *Lembaran Publikasi Minyak dan Gas Bumi*, 59(3), pp. 17–50. https://doi.org/10.29017/LPMGB.59.3.1891.